AAPS Open

RESEARCH

Open Access

Formulation mitigations for particle formation induced by enzymatic hydrolysis of polysorbate 20 in protein-based drug products: insights from a full-factorial longitudinal study

Inn H. Yuk[1], Theo Koulis[2], Nidhi Doshi[1], Kathrin Gregoritza[3], Constanze Hediger[3], Vanessa Lebouc-Haefliger[3], Jamie Giddings[1] and Tarik A. Khan[3*]

Abstract

Hydrolytic degradation of the polysorbate 20 (PS20) surfactant in protein-based liquid formulations releases free fatty acids (FFAs), which can accumulate to form particles in drug products during real-time (long-term) storage. To identify formulation conditions that mitigate the risk of particle formation, we conducted a longitudinal study using purified recombinant monoclonal antibody (mAb) formulated in 24 conditions. In this real-time stability study at 5 °C, three key formulation parameters—mAb concentration, initial PS20 concentration, and pH—were varied across representative ranges in a full-factorial design. A longitudinal regression analysis was used to evaluate the effects of these parameters and their interactions on PS20 degradation (via measurements of PS20, FFAs, and PS20 ester distribution) and on particle formation (via visible particle observations and subvisible particle counts). The time-dependent onset of visible particles trended with the rise in subvisible particle counts and FFA levels and fall in PS20 concentration. In the ranges studied here, lower mAb concentration and higher initial PS20 concentration delayed the onset of particles, whereas pH had a negligible effect. These observations were consistent with the general trends predicted by our previously published FFA solubility model. Taken together, these findings highlight the complex relationships between formulation parameters, PS20 degradation, and particle formation.

Keywords: Free fatty acids, Formulation design, Particles, Polysorbate degradation, Stability, Statistical analysis

Introduction

Polysorbate 20 (PS20) and polysorbate 80 (PS80) are the predominant surfactants used in biopharmaceutical formulations (Gervasi et al. 2018; Strickley and Lambert 2021). These non-ionic surfactants stabilize and protect the drug product (DP) against protein aggregation from interfacial stresses encountered during processing, transport, and administration (Khan et al. 2015). Both PS20 and PS80 are highly non-homogenous mixtures that demonstrate heterogeneity at multiple levels, such as fatty ester distribution and degrees of esterification (Hewitt et al. 2011). Unfortunately, PS20 and PS80 can

*Correspondence: tarik.khan@roche.com

[3] Pharma Technical Development Europe, F. Hoffmann-La Roche Ltd., Grenzacherstrasse 124, 4070 Basel, Switzerland
Full list of author information is available at the end of the article

degrade via oxidation and/or hydrolysis (Dwivedi et al. 2018; Jones et al. 2018). Although PS20 may be less prone to oxidation than PS80 (Kishore et al. 2011b; Schmidt et al. 2020; Yao et al. 2009), it is similarly susceptible to hydrolytic degradation (Kranz et al. 2019; Roy et al. 2021).

Polysorbate degradation observed in DP over real-time (long-term) storage is usually attributed to the presence of residual host cell proteins (HCPs) that are capable of enzymatically hydrolyzing the ester bond (Hall et al. 2016; Zhang et al. 2020, 2021, 2022b) to release free fatty acids (FFAs) as degradants (Dixit et al. 2016; Graf et al. 2021). In DPs formulated with polysorbate, the accumulation of sparingly soluble FFAs—such as lauric acid (LA), myristic acid (MA), and palmitic acid (PA) from PS20 hydrolysis, or oleic acid (OA), PA, and stearic acid (SA) from PS80 hydrolysis—can trigger undesirable particle phenomenon when the FFAs exceed their solubility limits (Doshi et al. 2015; Glücklich et al. 2020). Specifically, the FFAs can nucleate to form subvisible and visible populations of FFA particles (Cao et al. 2015; Saggu et al. 2015, 2021).

Hydrolytic degradation of the polysorbate surfactant to form FFA particles impacts DP critical quality attributes (CQAs). Parenteral DPs are required to be "practically free" or "essentially free" from visible particles (VPs) as per European Pharmacopoeia (Ph. Eur.) 2.9.20 and United States Pharmacopoeia (USP) <790>, respectively. Parenteral DPs are also required to meet cumulative subvisible particle (SVP) counts as per Ph. Eur. 2.9.19 and USP <787>. Furthermore, particles in DPs may be associated with potential adverse events (Carpenter et al. 2009; Doessegger et al. 2012). Therefore, DPs for parenteral use should consider VPs and SVPs as CQAs. Polysorbate content is also an important quality attribute for DP stability because the intact surfactant remaining at the end of shelf-life should still confer the desired protection from interfacial stresses (Kishore et al. 2011a; Pegues et al. 2021).

In recent years, the biopharmaceutical industry has increasingly reported incidences of and investigations into the root cause of polysorbate degradation and associated particle formation in protein formulations, particularly for recombinant monoclonal antibody (mAb) products (Allmendinger et al. 2021; Doshi et al. 2021; Graf et al. 2021; Gregoritza et al. 2022; Roy et al. 2021; Zhang et al. 2022a, 2022b, 2021, 2020). We hypothesize that this increasing prevalence of particle observations is the unintended consequence of multiple end-to-end aspects of current industry trends: (1) The reliance on intensified upstream processes to increase cell mass and productivity, which increases the HCP load and product recovery burden for downstream processing (Strube et al. 2018; Valente et al. 2018). (2) The shift to using chromatography steps with higher column load densities and/or preference for flow-through over bind-and-elute mode to increase downstream processing efficiency (Ichihara et al. 2018, 2019; Xu et al. 2020). (3) The emerging DP trends to meet demands for formulating at higher product concentrations, especially for subcutaneous and ocular administration of mAbs in chronic treatments (Gervasi et al. 2018; Page et al. 2022). These industry trends are expected to elevate residual HCP levels in the DP and thereby elevate both the extent of polysorbate degradation (from enzymatic hydrolysis) and the associated risk of FFA particle formation.

From a DP formulation perspective, for a given recombinant protein product, a higher DP concentration is projected to correlate with higher concentrations of residual hydrolytic HCPs. In a landmark report on PS80 hydrolysis and particles in mAb DP, Labrenz (2014) showed that FFA accumulation, which is indicative of hydrolytic polysorbate degradation, trended positively with mAb concentration ([mAb]) and PS80 concentration ([PS80]) (Labrenz 2014). More recently, Roy et al. showed that higher PS20 concentration ([PS20]) in a mAb formulation increased FFA accumulation but delayed SVP formation (Roy et al. 2021). However, there remains a paucity of DP studies that analyze the complex relationships between [mAb], polysorbate content, and other formulation parameters (such as pH) that can impact the accumulation and solubility of FFAs on VP and SVP formation.

There is a need for a comprehensive analysis of DP formulation parameters for their impact on polysorbate degradation and particle formation—both of which represent important DP stability attributes and can impact DP CQAs. In particular, there is a specific need to combine state-of-the-art analytics with Design of Experiments (DoE) methodologies to quantify the effects of multiple formulation parameters (as well as their interactions) on these important DP stability attributes under representative long-term storage conditions (i.e., 2–8 °C). Such statistical approaches can systematically identify and rank formulation designs to mitigate polysorbate degradation and the associated risk of FFA particle formation.

To address these current knowledge gaps, test specific hypotheses, and define formulation strategies for controlling DP CQAs, a longitudinal (i.e., time-course) study with PS20-containing mAb formulations was performed here as illustrated schematically in Fig. 1. In this longitudinal study, repeated measurements of the same attributes were made at multiple points in time over the course of the experiment. By including duration as a variable of interest in the resulting longitudinal model, the rate of change of an attribute (i.e., taken as a derivative

with respect to time) was also assessed (Fitzmaurice et al. 2011).

Three key formulation parameters—[mAb], initial [PS20], and pH—were tested using a full-factorial design to enable statistical analysis of their effects on multiple attributes. These parameters were selected for their potential impact on liquid DP stability in terms of PS20 hydrolytic degradation and FFA particle formation: (1) [mAb] is hypothesized to correlate positively with hydrolytic HCP concentration and hence the resulting extent of PS20 enzymatic hydrolysis and FFA accumulation, as indicated by a prior PS80 investigation (Labrenz 2014). (2) Initial [PS20] is hypothesized to affect FFA solubility and FFA precipitation through opposing mechanisms; at higher [PS20], its enhanced FFA-solubilizing capacity (Doshi et al. 2015, 2020) is potentially counteracted by elevated FFA generation from the larger PS20 substrate pool available for enzymatic hydrolysis (Roy et al. 2021). (3) pH is expected to affect FFA solubility and thereby influence the propensity for FFAs to precipitate, albeit to varying extents depending on the specific FFA and pH range, as illustrated in our previously published FFA solubility model (Doshi et al. 2015, 2020) and confirmed by Glucklich et al. (Glücklich et al. 2020). Differences in pH optimum for hydrolytic enzyme activity (Bhargava et al. 2021) may affect the rates of enzymatic PS20 hydrolysis and hence the resulting FFA accumulation. The impact of varying other typical formulation excipients, such as buffering agents and stabilizers, was not investigated here because of the lack of compelling hypotheses for their impact on FFA particle formation in DP over real-time stability. The statistical analysis of the longitudinal study outcomes—acquired from complementary, orthogonal analytical techniques—shed new insights into the complex time-dependent relationship between polysorbate degradation and particle formation as a function of three key formulation parameters within a pharmaceutically relevant design space.

Materials and methods

Reagents and materials

Recombinant mAb X is an IgG1-based mAb produced in-house (Roche, Penzberg, Germany) from recombinant CHO cells and purified using Protein A affinity followed by two ion-exchange chromatography steps. L-Histidine and histidine-HCl were purchased from Ajinomoto Aminoscience LLC. L-Methionine and sucrose were obtained from S.A. Ajinomoto Omnichem N.V and Ferro Pfanstiehl, respectively. High Purity™ polysorbate 20 was purchased from Croda Inc. Water for injection was produced in-house using a multi-stage pressure column distillation unit (Bosch Pharmatec).

Study set up

For the preparation of mAb X DP formulations, purified mAb X solution (Roche, Penzberg, Germany) provided

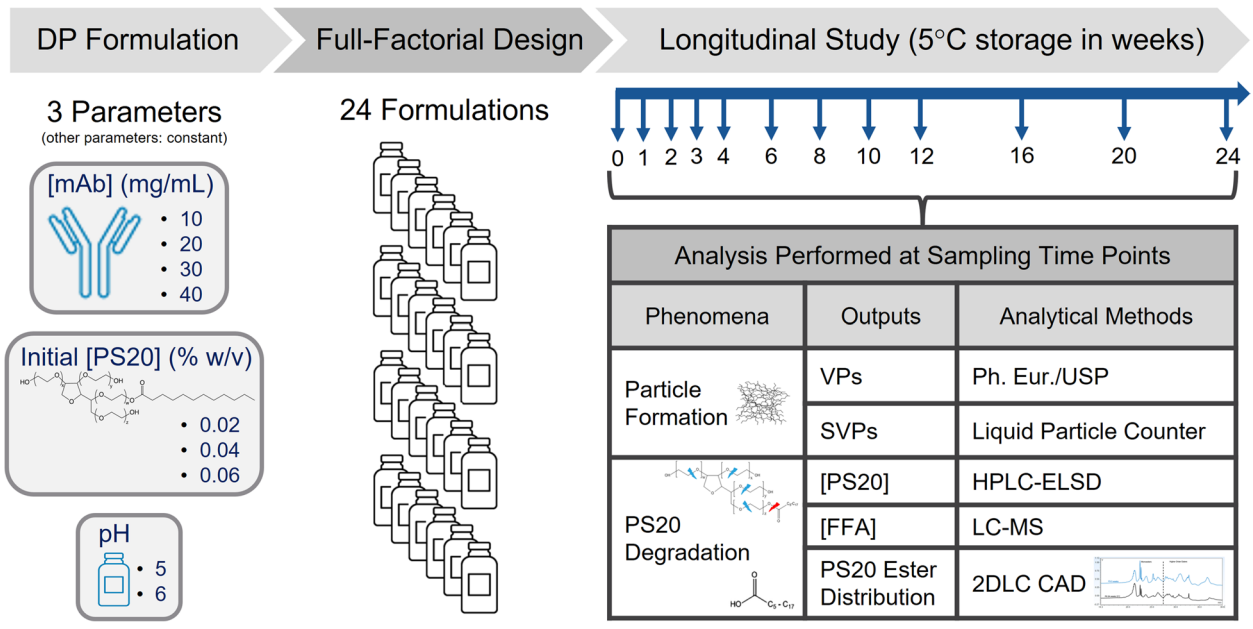

Fig. 1 DP stability study design to assess the impact of three formulation parameters on particle formation and PS20 degradation. The 24 DP formulations of mAb X—differing in [mAb], initial [PS20], and pH—were stored in glass vials at 5 °C and monitored using complementary/orthogonal analytical methods for particle formation and PS20 degradation over 24 weeks

in 20 mM histidine buffer (pH 6) was buffer exchanged and concentrated via ultrafiltration/diafiltration (UFDF) to ~ 60 mg/mL with 20 mM histidine-HCl buffer at pH 5.0 or 6.0. The molecular weight cutoff for the UFDF membranes used was 30 kD. The 24 formulations listed in Table 1 used varying concentrations of mAb X and high purity polysorbate 20 (Croda International), keeping the amounts of sucrose (200 mM) and L-methionine (10 mM) constant in all formulations. These formulations were prepared by using either pH 5.0 or 6.0 20 mM histidine-HCl buffer for dilution buffers and stock solutions, as appropriate. The pH and mAb content of all solutions were verified using a pH meter and an ultraviolet–visible spectrophotometer at 280-nm absorbance, respectively. Sample solutions were filtered through 0.22-µm porosity filter cartridges (Sterivex-GV, Millipore) and 1.5-mL aliquots of the sterile bulk formulation were transferred into 2 cc borosilicate glass vials (Fiolax®, Schott). Vials were sealed with bromobutyl teflonized and siliconized D777-1 stoppers (Daikyo Seiko Ltd.) and closed with aluminum crimped caps. Samples were stored at 5 °C for up to 24 weeks and analyzed as described below. The containers selected for PS20-related analytics were taken randomly. For light obscuration, if a sample in a given formulation/time point showed visible FFA particles while other containers in the same condition did not, the same sample containing particles was used for SVP analysis.

Analytical methods

Particle analysis

For VP analysis, three vials per formulation were assessed at each time point after equilibration to ambient temperature. Visual inspection was performed according to the Ph. Eur. 2.9.20/USP < 790 > method using a black and white panel by a single analyst. A positive visual inspection result was recorded for the presence of FFA particles when at least one of the three vials inspected per formulation per time point contained > 7 particles, based on visual appearance consistent with FFA particles. The real-time storage duration until the onset of visible FFA particles (VP-free duration) was used as an analysis parameter for statistical analysis.

Cumulative SVP counts were determined from one vial per formulation per time point for four size categories (≥ 2 µm, ≥ 5 µm, ≥ 10 µm, and ≥ 25 µm), assessed by light obscuration after equilibration to ambient temperature based on the principles of USP < 787 >, < 788 >, and < 789 >, using a HIAC 9703 + liquid particle counting system equipped with a 3000A sampler and HRLD-150 sensor (Hach). The instrument performance was verified using 5 µm COUNT-CAL™ count precision size standards (Thermo Scientific). Four 0.2-mL aliquots were sampled for each measurement, and the results of the last three aliquots were used to generate the average cumulative SVP count. The instrument used is rated for SVP concentrations up to 18,000 particles/mL. Since some of the measurements exceeded this limit, the time duration of remaining at low SVP concentration (i.e., low SVP duration) was used instead of the continuous variable of SVP concentration for statistical analysis.

PS20 quantitation

Intact PS20 content was determined from one vial per formulation per time point by mixed mode high-performance liquid chromatography (HPLC) equipped with evaporative light scattering detector (ELSD) based on a method developed by Hewitt et al. (Hewitt et al. 2008), with modifications described in Doshi et al. (Doshi et al. 2020). Fluorescence micelle assay (FMA) was not used for quantifying intact PS20 content because of FMA limitations observed in head-to-head comparisons against HPLC-based methods (Lippold et al. 2017). Those comparisons indicated that FMA was not able to detect polyoxyethylene sorbitan monolaurate, the main component of PS20, at the tested concentration.

FFA quantitation

FFA concentration ([FFA]) for LA, MA, PA, and SA were determined from one vial per formulation per time point by liquid chromatography-mass spectrometry (LC–MS) as detailed by Honemann et al. (Honemann et al. 2019).

PS20 ester distribution

PS20 ester distribution was determined for select formulations and conditions using a modified version of the method developed by Li et al. on a two-dimensional liquid chromatography (2DLC) system coupled to a Thermo Corona Ultra charged aerosol detector (CAD) (Li et al. 2014). The first dimension was conducted on a mixed-mode column to remove the mAb. The PS20-containing eluate from the first dimension was flowed onto a reversed phase column in the second dimension to separate the PS20 ester subspecies. The first dimension utilized the following: an Oasis MAX column (20 mm × 2.1 mm, 30 µm); 0.2% formic acid in water as mobile phase A; 0.2% formic acid in acetonitrile as mobile phase B; gradient of 0–3.0 min, 20% B; 3.0–3.1 min, 20–90% B; 3.1–8.1 min, 90% B; 8.1–8.2 min, 90–20% B; 8.2–13.2 min, 20% B at a flow rate of 1.0 mL/min. The second dimension utilized the following: an Acquity BEH C18 column (150 mm × 2.1 mm, 1.7 µm); 0.05% formic acid in water as mobile phase A; 0.04% formic acid in acetonitrile as mobile phase B; gradient of 0–30.0 min, 15–100% B; 30.0–35.0 min, 100% B; 35.0–35.1 min, 100–15% B; 35.1–40.0 min, 15% B at a flow rate of 0.5 mL/min. The

Table 1 VP observations in the longitudinal study with a full-factorial design to assess the impact of three formulation parameters. The 24 mAb X DP formulations—differing in [mAb], initial [PS20], and pH—were stored at 5°C and monitored for VPs over 24 weeks. Three glass vials per formulation were visually inspected for VPs at each of 12 time points according to the Ph. Eur./USP method

Formulation	pH	Initial [PS20] (% w/v)	[mAb] (mg/mL)	VP observations (weeks)											
				0	1	2	3	4	6	8	10	12	16	20	24
F1	5.0	0.02	40	no	no	no	yes	yes	yes	yes	yes	yes	yes	yes	yes
F2			30	no	no	no	no	yes	yes	yes	yes	yes	yes	yes	yes
F3			20	no	no	no	no	no	yes	yes	yes	yes	yes	yes	yes
F4			10	no	no	no	no	no	no	no	yes	yes	yes	yes	yes
F5		0.04	40	no	no	no	no	no	yes	yes	yes	yes	yes	yes	yes
F6			30	no	no	no	no	no	yes	yes	yes	yes	yes	yes	yes
F7			20	no	no	no	no	no	no	no	no	no	yes	yes	yes
F8			10	no	no	no	no	no	no	no	no	no	no	yes	yes
F9		0.06	40	no	no	no	no	no	no	yes	yes	yes	yes	yes	yes
F10			30	no	no	no	no	no	no	no	yes	yes	yes	yes	yes
F11			20	no	no	no	no	no	no	no	no	no	yes	yes	yes
F12			10	no	no	no	no	no	no	no	no	no	no	no	yes
F13	6.0	0.02	40	no	no	no	yes	yes	yes	yes	yes	yes	yes	yes	yes
F14			30	no	no	no	no	yes	yes	yes	yes	yes	yes	yes	yes
F15			20	no	no	no	no	no	yes	yes	yes	yes	yes	yes	yes
F16			10	no	no	no	no	no	no	no	no	no	yes	yes	yes
F17		0.04	40	no	no	no	no	no	yes	yes	yes	yes	yes	yes	yes
F18			30	no	no	no	no	no	yes	yes	yes	yes	yes	yes	yes
F19			20	no	no	no	no	no	no	no	no	no	yes	yes	yes
F20			10	no	no	no	no	no	no	no	no	no	no	yes	yes
F21		0.06	40	no	no	no	no	no	no	yes	yes	yes	yes	yes	yes
F22			30	no	no	no	no	no	no	no	no	no	yes	yes	yes
F23			20	no	no	no	no	no	no	no	no	no	yes	yes	yes
F24			10	no	no	no	no	no	no	no	no	no	no	no	no

% higher order ester peak area was calculated relative to the total peak area consisting of the monoester and higher order (di- and tri-) ester peaks of PS20.

Statistical analysis

The longitudinal study consisted of a full-factorial experiment in three factors: (1) [mAb] was tested at 4 levels: 10, 20, 30, and 40 mg/mL; (2) initial [PS20] was tested at 3 levels: 0.02, 0.04, and 0.06% w/v; and (3) pH was tested at 2 levels: 5 and 6. The full-factorial design yielded 24 unique DP formulations that were measured longitudinally at regular intervals (as depicted in Fig. 1 and detailed in Table 1).

Longitudinal data (intact [PS20] and [LA]) from the resulting full-factorial longitudinal study were analyzed using a mixed-effects regression model in order to obtain estimates of PS20 degradation rates and to account for repeated measurements over each formulation. The mixed-effects model was fitted using restricted maximum likelihood (REML) (Pinheiro and Bates 2000). All regression analyses were performed using JMP 16 (SAS Institute).

The longitudinal analysis of the data was performed by fitting a mixed-effects regression model that included the following fixed effects: the main effects for the three factors, their two-way interactions and three-way interaction, time, and all time-crossed terms (time × factors and time × interactions). In order to account for the repeated measurements, formulation was included as a random effect:

$$\begin{aligned} Y = {} & [\textit{factors}] + [\textit{two-way interactions}] \\ & + [\textit{three-way interaction}] + [\textit{time}] \\ & + [\textit{time} \times \textit{factors}] + [\textit{time} \times \textit{two-way interactions}] \\ & + [\textit{time} \times \textit{three-way interaction}] \\ & + [\textit{formulation}] + \textit{error} \end{aligned} \quad (1)$$

This design-appropriate regression model allowed the simultaneous fitting of the longitudinal data and the PS20 degradation rate. The fitted model for the PS20 degradation rate was obtained by taking a time derivative of the fitted mixed-effects regression. In this way, the fitted model for the degradation rate included the main effects for the three factors and all interactions. Because the study design followed a full-factorial longitudinal design, the estimates of the fixed effects were uncorrelated, so that model reduction was not necessary.

Similarly, non-longitudinal data (VP-free duration and low SVP duration) were analyzed by fitting a linear

regression model that included the main effects for the three factors, their two-way interactions, and the three-way interaction:

$$Y = [factors] + [two\text{-}way\ interactions] + [three\text{-}way\ interaction] + error \quad (2)$$

To facilitate comparisons among effect estimates, the three factors were scaled (coded) so that all the coefficients (effect estimates) of the fitted regressions have the units of the response (or derivative). The use of coded variables in the regression analysis enabled the largest effect estimates to be identified and ranked.

Results and discussion

Study design and rationale

Recombinant mAb X was selected for this formulation study because its liquid DP underwent rapid PS20 hydrolysis and generated VPs relatively quickly (i.e., within weeks/months) in real-time stability studies at 5 °C, as shown by our earlier investigations into mAb B (Doshi et al. 2021), which is referred to as mAb X herein. The CHO-derived mAb X material was produced using upstream and downstream processes that were representative of typical large-scale mAb manufacturing. The VPs isolated by gold filter were previously characterized as FFAs by LC–MS and FTIR microscopy for mAb B (Doshi et al. 2021), which is the mAb X studied here. There were no signs of oxidative PS20 degradation by GC–MS (data not shown); furthermore, the mAb X DP formulations studied here included 10 mM L-methionine, which is known to mitigate oxidative degradation of PS20 (Doshi et al. 2021). Therefore, mAb X served as a relevant model for studying the impact of formulation parameters on PS20 hydrolysis and FFA particle formation under representative long-term DP storage conditions (2–8 °C). By conducting our formulation studies at 5 °C and at pH 5–6, chemical hydrolysis of PS20 was considered negligible (Dwivedi et al. 2020; Kishore et al. 2011b). In light of how the complex phenomenon of FFA particle nucleation for DP stored at different temperatures can exhibit distinct, perplexing differences (Roy et al. 2021), our study of mAb X formulations at 5 °C storage circumvents accelerated or stress conditions—and the associated limitations in interpreting or extrapolating the results to actual DP storage conditions. Based on the totality of evidence provided above, the PS20 degradation observed in mAb X formulations in this study can be attributed to enzymatic hydrolysis and not chemical hydrolysis. Specifically, all mention of PS20 hydrolysis or hydrolytic degradation hereafter imply an underlying mechanism that is enzymatic in nature with residual CHO-derived HCPs as the root cause.

This longitudinal DoE study (as depicted in Fig. 1 and detailed in Table 1) was designed with the following rationale: (1) [mAb] was tested at 4 levels because of its hypothesized significant impact on PS20 hydrolysis and associated FFA particle formation as well as the lack of DoE studies with this parameter apart from the PS80 study by Labrenz (Labrenz 2014); (2) initial [PS20] was tested at 3 levels because of its predicted impact on PS20 hydrolysis and FFA particle formation (Doshi et al. 2015, 2020; Roy et al. 2021); and (3) pH was tested at 2 levels because of its projected lesser impact on FFA particle formation in the tested pH range according to our FFA solubility model (Doshi et al. 2015, 2020) while addressing potential impact from different pH optimum for hydrolytic enzyme activity (Bhargava et al. 2021). The values tested for these formulation parameters were additionally designed to fall within the typical ranges reported for [mAb], initial [PS20], and pH in liquid parenteral DPs (Falconer 2019; Gervasi et al. 2018; Strickley and Lambert 2021). For example, in a recent survey of commercially available antibody formulations (Strickley and Lambert 2021), 97 out of 113 formulations used pH 5–6, which is the pH range selected for this study. The values for the initial [PS20] and pH were also designed to fall within the ranges previously established for our FFA solubility model (Doshi et al. 2015, 2020). The [mAb] and time points for analyses were selected based on prior VP observations in which the mAb X studied here was referred to as mAb B in the earlier studies (Doshi et al. 2021). The outputs selected for this formulation study were generated using state-of-the-art analytical methods that are orthogonal/complementary in nature for studying particle formation and PS20 degradation (Fig. 1). Particle formation was evaluated using two different approaches: Ph. Eur./USP method for VPs and HIAC liquid particle counter for monitoring cumulative SVP counts. PS20 degradation was evaluated using three orthogonal analytical methods to quantify: (1) intact PS20; (2) FFAs, the main degradants from PS20 hydrolysis; and (3) PS20 ester distribution.

Particle formation

Visible particles (VPs)

Both [mAb] and initial [PS20] impacted the timing observed for the onset of VPs in the different mAb X formulations (Table 1). Lower [mAb] and higher initial [PS20] extended the VP-free duration (Fig. 2). These observations are consistent with previously observed directionality of [mAb] (Labrenz 2014) and initial [PS20] (Roy et al. 2021) on FFA generation rates and consequently FFA particle formation. The VP results were similar between pH 5 and pH 6 samples (Fig. 2 and Table 1),

with a marginal benefit at pH 6, consistent with our projections based on the minimal predicted positive impact of higher pH in this range on PA solubility using our previously published FFA model (Doshi et al. 2015, 2020).

All samples were aligned in their presence or absence of FFA VPs across the 3 containers analyzed for each time point except for 6 analyses out of 288 analyses (from 12 time points for 24 cases). Five of the 6 analyses [in which each analysis used 3 containers] showing some containers with FFA particles and some without were at the time point at which the formulation began to show particles, and 1 (F20) showed mixed results across the containers at the last time point at 24 weeks. These mixed results in a small fraction of the 288 analyses (~2%) are not surprising given that they occurred around the time of particle onset and particle formation is a probabilistic event.

Of the 24 formulations tested, the only formulation (F24; Table 1) that remained free of VPs throughout the 24-week DP stability study contained the highest initial [PS20] (0.06% w/v) and lowest [mAb] (10 mg/mL) at pH 6. The VP observations highlight the time-dependent and non-transient nature of VP formation in the mAb X formulations—for any given formulation, after the first time point with VPs detected, all subsequent time points of that formulation were also positive for VP observations (Table 1). These VP observations are consistent with our understanding of the nature of FFA particles—PS20 hydrolysis results in the accumulation of FFAs over time (Saggu et al. 2021; Tomlinson et al. 2015); once the FFA levels exceed their solubility limits, the FFAs precipitate to form VPs (Doshi et al. 2015, 2020).

Subvisible particles (SVPs)

Both [mAb] and initial [PS20] impacted the SVP count profiles in the different mAb X formulations (Fig. 3; Supplementary Figs. S1, S2, and S3). The formulations with the lowest [mAb] consistently showed the lowest SVP counts (in all four size categories) across all time points; the formulations with the highest initial [PS20] tended to show a delayed increase in SVP counts. SVP count profiles across the SVP size categories displayed similar trends across the three smaller size categories ($\geq$2-µm, $\geq$5-µm, and $\geq$10-µm particles) as shown in Fig. 3 and Supplementary Figs. S1 and S2. By contrast, the particle count profiles for the largest size category ($\geq$25-µm particles) showed minimal (0.2% w/v PS20) or delayed (0.4% and 0.6% w/v PS20) increase in counts with time relative to the other size categories (Supplementary Fig. S3).

The colored asterisks in Fig. 3 and Supplementary Figs. S1, S2, and S3 (with colors matching the corresponding [mAb] in the formulation) denote the earliest time point with VPs observed for each formulation. Although the onset of VPs occurred close to the rise in SVP counts in some formulations, there are some notable exceptions: (1) the formulations with the lowest [mAb] continued to show low SVP counts across all size categories even after the onset of VPs, and (2) the largest size category for SVP counts ($\geq$25 µm) continued to stay low (<50 particles/mL) for weeks after the onset of VPs, especially for the formulations with the lowest initial [PS20].

Based on the findings here and considerations elsewhere on the application of SVPs in the 2–100-µm size range (Carpenter et al. 2009; Corvari et al. 2015), the data from the smallest SVP size category ($\geq$2 µm) were further analyzed for the impact of formulation parameters. A low SVP count threshold (<350 particles/mL) was applied based on in-house experience to approximate the onset of the rise in SVP counts above background noise (Gregoritza et al. 2022). Lower [mAb] and higher initial [PS20] extended the storage duration with low SVP counts (Fig. 4), similar to the directionality of their effect on the storage duration with no VPs (Fig. 2). By contrast, formulation pH did not show a notable impact on the SVP count profiles (Fig. 3; Supplementary Figs. S1, S2, and S3) or on the duration with low SVP counts (Fig. 4).

Correlations between visible and subvisible particles

The precise dynamics behind the complex phenomenon of FFA particle formation in DP has not been defined. We hypothesized that FFA accumulation would lead to SVPs that eventually grow in size until they exceed the visual detection threshold and are observed as VPs during visual inspection. To test our simplistic FFA nucleation hypothesis, the 24 mAb X formulations were analyzed for potential trends between SVPs and VPs over storage duration. The plot of VP-free duration against low SVP count duration (Fig. 5) yielded a strong positive correlation (coefficient of determination, $R^2 = 0.89$). The slope of this linear regression (0.84), being lower than one, indicated that the rise in SVP counts did not tend to precede the onset of VPs. The SVP count profiles did not indicate that the SVPs progressively grew in size with DP storage time for any given formulation (Fig. 3; Supplementary Figs. S1, S2, and S3).

Taken together, these observations for the particle phenomenon in mAb X formulations over 5 °C storage contradict our FFA nucleation hypothesis that a rise in SVP counts would precede—and thereby forecast—the subsequent onset of VPs in DP stability studies. However, they do support a positive trend between the rise in SVP counts and the onset of VPs for mAb X DP. Given the complexity of the particle nucleation phenomenon (Allmendinger et al. 2021; Gregoritza et al. 2022; Roy

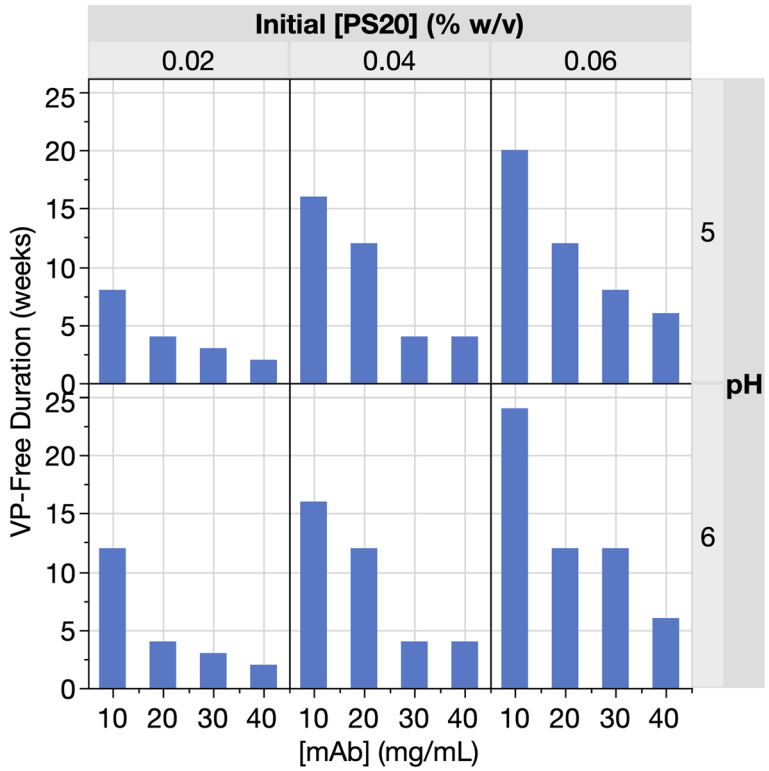

Fig. 2 Storage duration without VPs observed for mAb X DP as a function of [mAb]. The 24 formulations (listed in Table 1) represent unique combinations of [mAb], initial [PS20], and pH. At the end of the DP stability study (24 weeks at 5 °C), only one formulation (F24 as shown in Table 1) remained free from VPs

et al. 2021; Saggu et al. 2021), and the relatively early onset of particles in the mAb X formulations, the overall trends between SVPs and VPs observed here may not be generalizable.

Polysorbate degradation

PS20 concentration ([PS20])

Both [mAb] and initial [PS20] impacted PS20 degradation in the different mAb X formulations (Fig. 6). Across the 24 formulations, [PS20] decreased over storage time at 5 °C in a relatively linear manner, with the following exceptions: (1) two formulations at pH 5 and pH 6 (F1 and F13) with the highest [mAb] and lowest initial [PS20] and (2) the next two formulations with the second highest [mAb] (F2 and F14) and lowest initial [PS20], albeit to a lesser extent. These four formulations exhibited a leveling of intact [PS20] after ~ 10 weeks.

There are several potential underlying mechanisms that can cause a time-dependent decrease in the rate for enzymatic hydrolysis of PS20 in DP over real-time stability studies: (i) PS20 substrate limitation, (ii) diffusion limitation, and (iii) enzyme inhibition/inactivation. The time-course profiles for the F1, F2, F13, and F14 formulations show the lowest intact [PS20] relative to other formulations by ~ 10 weeks at 5 °C storage, thereby indicating potential limitations in PS20 substrate availability. The ratio of residual hydrolytic HCPs to their preferred PS20 substrates should be highest in the formulations with the highest [mAb] and lowest [PS20]—F1 and F13, followed by F2 and F14, are thereby expected to show enzyme exhaustion of PS20 substrate ahead of the other formulations. In theory, PS20 hydrolysis in mAb X formulations would cease upon depletion of the specific type(s) of PS20 substrate utilized by the residual PS20-degrading enzyme(s), leading to an eventual flattening in the decline of the [PS20] over storage duration. In addition, if the theory of diffusion-controlled hydrolysis reaction observed in other systems (Guha et al. 1988) applies to PS20 hydrolysis, when [PS20] drops to a sufficiently low level during the static conditions for the real-time DP stability study at 5 °C, diffusion constraints may limit the encounters of enzymes with PS20 substrate and thereby limit the reaction rate. Specifically, the rate of occurrence for the enzyme–substrate collision encounters required for enzymatic reaction is limited by diffusion (Bar-Even

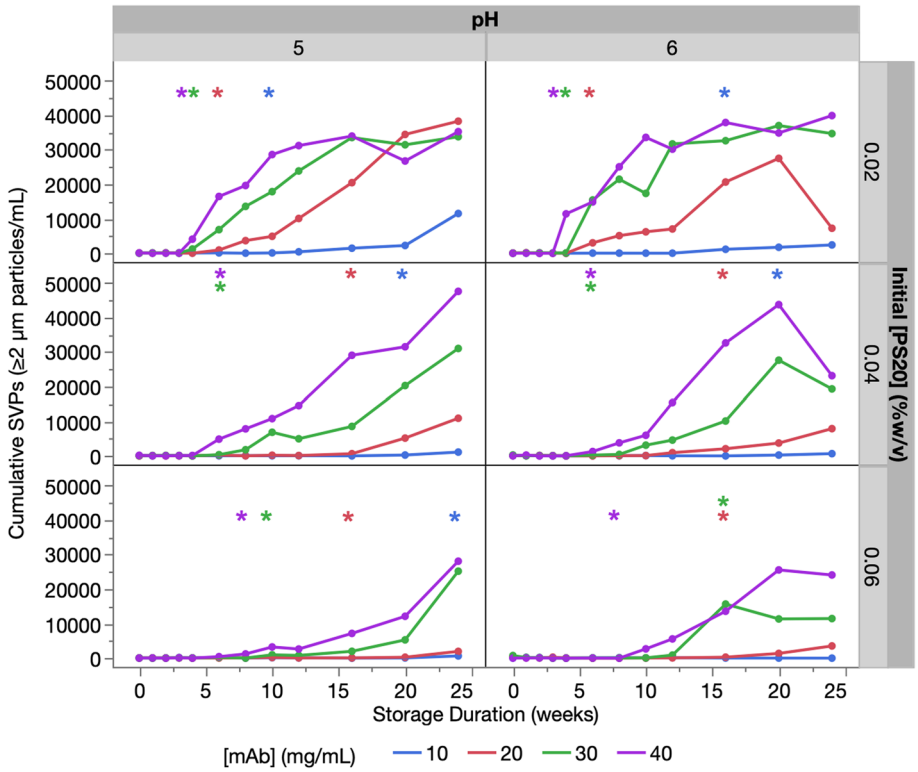

Fig. 3 Cumulative SVP counts (≥ 2 µm particles/mL) measured in mAb X DP over storage duration (weeks at 5 °C). Three formulation parameters—[mAb], initial [PS20], and pH—were assessed for their impact on SVP accumulation as measured by HIAC liquid particle counter. The 24 formulations and their VP outcomes are detailed in Table 1. Colored asterisks in the plots denote the earliest time points at which VPs were observed for the formulation (with corresponding [mAb] represented by the same color)

et al. 2015); the resulting reaction rate would therefore be expected to decrease at lower enzyme and substrate concentrations, consistent with Michaelis–Menten kinetics. Finally, although it has been shown FFAs can inhibit the activity of lipoprotein lipase (Bengtsson and Olivecrona 1980)—a hydrolytic HCP shown to degrade PS20 (Chiu et al. 2017)—it is unlikely that the accumulation of PS20 degradants is the predominant underlying mechanism for the slow down in PS20 hydrolysis observed for F1, F2, F13, and F14 formulations (Fig. 5). If enzyme inhibition/inactivation was occurring—whether because of accumulation of inhibitory PS20 degradants or for other reasons over DP storage—the formulations with higher amounts of PS20 degradation should also show decrease in PS20 hydrolysis over time. However, the formulations with higher initial [PS20] and higher extent of PS20 degradation do not show a notable decrease in PS20 hydrolysis. Therefore, the decline in PS20 degradation in F1, F2, F13, and F14 formulations is not ascribed to enzyme inactivation over DP storage or negative feedback on enzyme activity by end-product inhibition.

The concept of PS20 substrate limitation may be extended to incorporate the substrate specificity of residual HCPs that hydrolyze PS20; different hydrolytic enzymes may have different preferences for PS20 substrates. For example, some enzymes preferentially degrade higher order (di- and tri) esters instead of monoesters; other enzymes preferentially degrade sorbitan instead of isosorbide species (Graf et al. 2020; McShan et al. 2016; Zhang et al. 2022b). The time-course profiles for PS20 ester distribution corroborate our hypothesized enzyme selectivity towards specific PS20 substrates; all tested formulations showed preferential higher order ester degradation in PS20 over storage time at 5 °C as shown by representative chromatograms (Supplementary Fig. S4). Similar to the time-course profiles for intact [PS20], the % higher order ester peak area also leveled off in the formulations with the lowest initial [PS20] (0.02% w/v) and highest [mAb] (40 mg/mL) after ~ 10 weeks (Supplementary Fig. S5). These observations support our hypothesis that the preferred substrate (i.e., higher order PS20 ester species) by the enzymes in the mAb X formulations were depleted in

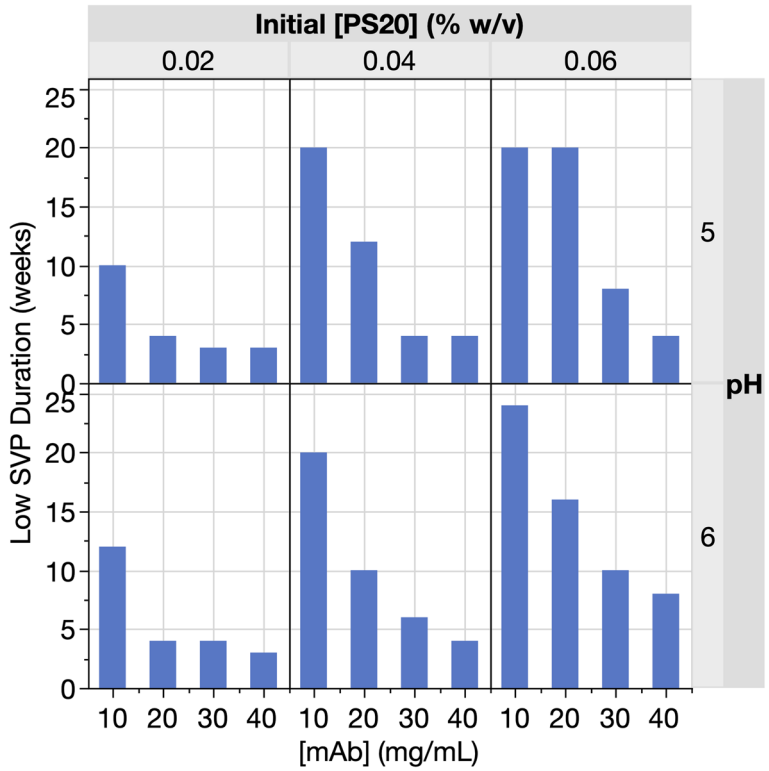

Fig. 4 Storage duration with low SVP counts in mAb X DP as a function of [mAb]. The 24 formulations were stored at 5 °C and represent unique combinations of [mAb], initial [PS20], and pH as listed in Table 1. For each formulation, the duration with low cumulative SVPs (< 350 counts for ≥ 2 µm particles/mL) was determined by SVP measurements (using HIAC liquid particle counter) at 12 time points over 24 weeks

these formulations. By contrast, the formulations with higher initial [PS20] (0.04% and 0.06% w/v) and the lowest [mAb] (10 mg/mL) had a relatively linear decrease in % higher order ester peak area over time.

By taking the time derivative from the longitudinal model for the measured [PS20] output, the rate of change in [PS20] over time (d[PS20]/dt) was calculated for all the conditions (Fig. 7). The calculated absolute value of the rate of change of PS20 concentration with time (|d[PS20]/dt|) was taken to represent the rate of PS20 degradation. At the lowest [mAb], |d[PS20]/dt| was also the lowest, irrespective of the initial [PS20] in the formulation design. The consistently low |d[PS20]/dt| for formulations with the lowest [mAb] indicates that the hydrolysis has already achieved the maximum rate of enzymatic reaction at substrate saturation (V_{max})—PS20 hydrolysis is thereby rate-limited by enzyme availability (and not by PS20 substrate). By contrast, at the highest [mAb], |d[PS20]/dt| was not only higher but also increased with initial [PS20] in the formulation design. In the ranges tested, higher [mAb] and higher initial [PS20] both increased |d[PS20]/dt|, thereby indicating that the hydrolysis reaction continued to increase with enzyme concentration and [PS20]. Hence, PS20 hydrolysis can be limited by the availability of both enzyme and PS20 substrate, consistent with expectations from Michaelis–Menten enzyme kinetics (Bar-Even et al. 2015).

In contrast to [mAb] and initial [PS20], formulation pH did not have a notable impact on the PS20 degradation profile over storage time at 5 °C (Fig. 6). However, for formulations with identical [mAb] and initial [PS20], |d[PS20]/dt| was generally slightly higher for pH 6 compared to pH 5 (Fig. 7). The exceptions were formulations where the PS20 substrate is postulated to be limiting (F1, F2, F13, and F14) and slowed down the PS20 decline over storage duration (Fig. 6). These formulations also yielded the lowest measured [PS20] values over time, which is attributed to their combination of lowest initial [PS20] and higher [mAb]. The low [PS20] values measured in these formulations—especially during the final time points (where [PS20] < 0.01% w/v)—are closer to the limit of quantitation (LOQ) of the PS20 content method. Therefore, the out-of-trend calculated rates for F1 and F13, in which pH 6 showed marginally higher |d[PS20]/dt| than pH 5 (~ 10% difference), may reflect assay limitations (in terms of LOQ and method precision) instead of actual pH impact.

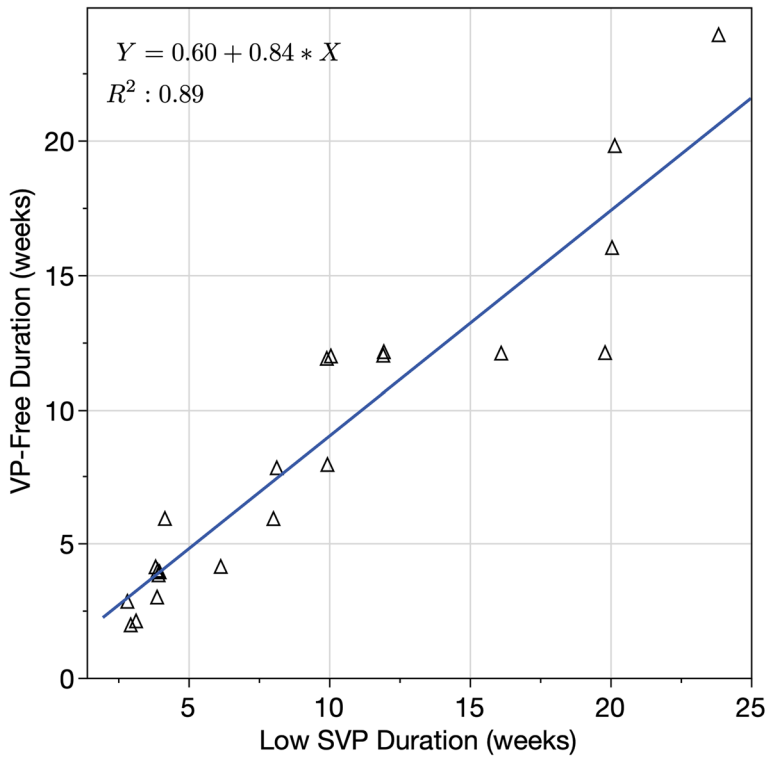

Fig. 5 Correlation between VP-free duration and low SVP duration for mAb X DP. The 24 formulations (listed in Table 1) were stored at 5 °C and represent unique combinations of [mAb], initial [PS20], and pH. Each formulation was monitored at 12 time points over 24 weeks for VPs (by the Ph. Eur./USP method) and cumulative SVP counts (≥ 2 µm particles/mL by HIAC liquid particle counter). SVP count threshold of < 350 particles/mL was used to determine the low SVP duration (in weeks)

The generally slightly higher |d[PS20]/dt| at pH 6 (Fig. 7) may be attributed to the activity of hydrolytic enzymes being marginally higher at pH 6 than pH 5. Some of the hydrolytic enzymes previously identified in mAb samples that are capable of degrading polysorbate (Chiu et al. 2017; Zhang et al. 2020) have optimum activities at higher pH: lipoprotein lipase prefers pH ~ 8 and higher (Bengtsson and Olivecrona 1982); carboxylesterases prefer ~ pH 6.5–8.0 (Imai 2006). In an in-house study using a different purified mAb, no discernible difference in esterase activity rates was observed between pH 5 and 6, but notably higher activity rates were observed at pH 8 (Bhargava et al. 2021). In theory, the impact of formulation pH on PS20 degradation in a given DP will depend on the specific residual PS20-degrading enzymes present and their optimum pH preference; the residual enzymes present in mAb X DP may not be representative of the residual enzymes present in other DPs and hence the pH findings here may not be generalizable to other DPs.

Lauric acid concentration ([LA])

PS20 is a heterogeneous mixture of fatty acid esters, of which laurate esters are the main species present at greater than 40% of the composition (Doshi et al. 2021) in compliance with Ph. Eur./USP specifications. Therefore, the main FFA degradant generated from PS20 hydrolysis is expected to be LA. Both [mAb] and initial [PS20] impacted [LA] in the different mAb X formulations (Fig. 8). [LA] increased over storage duration at 5 °C in a relatively linear manner across the majority of the 24 formulations. The following four formulations were exceptions and exhibited a plateau in [LA] after ~ 10 weeks: (1) two formulations (F1 and F13) at pH 5 and pH 6 with the highest [mAb] and lowest initial [PS20] and (2) the next two formulations (F2 and F14) with the second highest [mAb] and lowest initial [PS20], albeit to a lesser extent. These exceptions are the same four formulations highlighted earlier as showing a deceleration in the decline in intact [PS20] over time (Fig. 6). Taken together, the longitudinal data for intact [PS20] and [LA] show complementary corroborating trends on PS20 degradation within each formulation. For example, they highlight a deceleration in PS20 degradation over storage duration

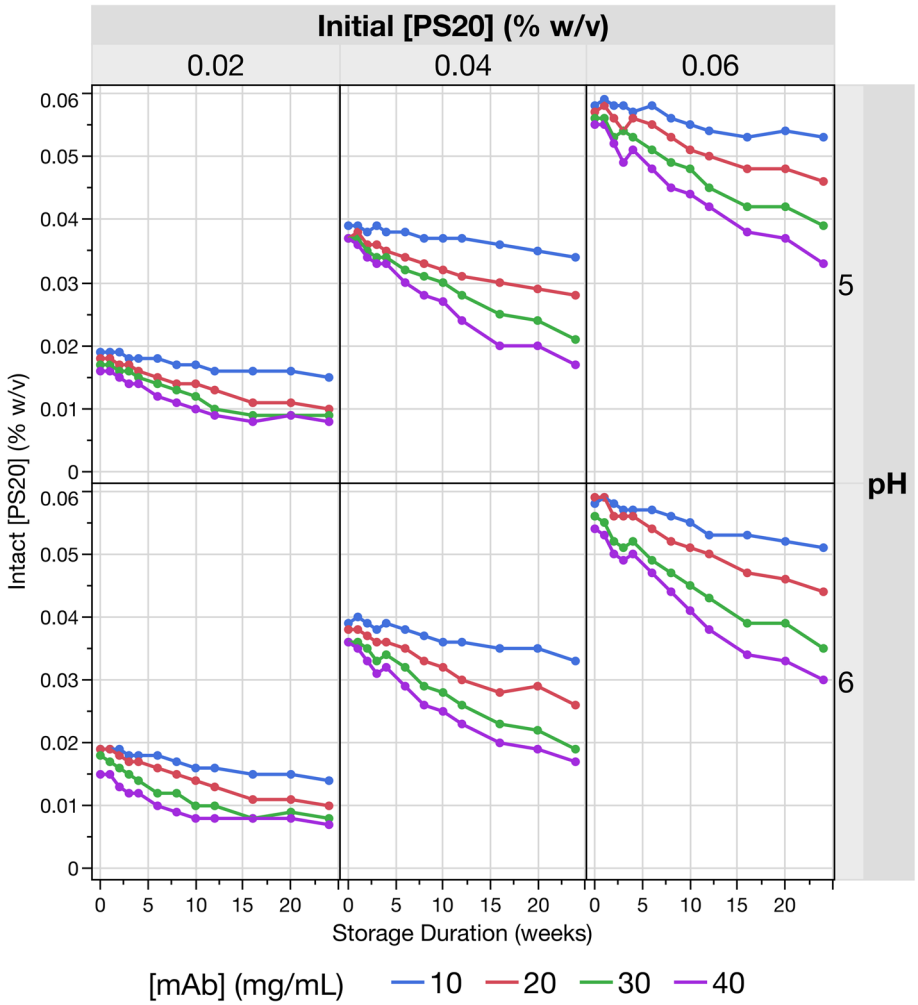

Fig. 6 Intact [PS20] in mAb X DP over storage duration (weeks at 5 °C). The 24 formulations (listed in Table 1) represent unique combinations of [mAb], initial [PS20], and pH. Intact [PS20] remaining at each time point was quantified by HPLC-ELSD

in the same four formulations (F1, F2, F13, and F14); this deceleration is attributed to enzyme exhaustion of certain higher order ester species of the PS20 substrate in those formulations (Supplementary Fig. S5), as discussed in detail in the previous section on PS20 concentration.

By taking the time derivative from the longitudinal model for [LA], the rate of change in LA concentration (d[LA]/dt) was calculated for all the formulations (Fig. 9). At the lowest [mAb], d[LA]/dt was also the lowest, irrespective of the initial [PS20] in the formulation design. The consistently low values of d[LA]/dt for formulations with the lowest [mAb] indicates that the hydrolysis reaction has already achieved V_{max}—PS20 hydrolysis is thereby rate-limited by enzyme availability (and not PS20 substrate). By contrast, at the highest [mAb], d[LA]/dt was not only higher but also increased with initial [PS20] in the formulation design. In the ranges tested, higher [mAb] and higher initial [PS20] increased d[LA]/dt. These findings corroborate the analyses of d[PS20]/dt (Fig. 7). For example, they highlight the highest |d[PS20]/dt| were observed in the formulations with highest [mAb] and highest initial [PS20] (F9 and F21) and hence the best availability of hydrolytic enzymes and PS20 substrate. Taken together, the longitudinal analyses for [PS20] (Figs. 6 and 7) and [LA] (Figs. 8 and 9) support our earlier discussions and conclusion that in the formulation ranges tested, enzymatic PS20 hydrolysis is limited by both enzyme and substrate availability through [mAb] and initial [PS20], respectively.

In contrast to [mAb] and initial [PS20], formulation pH exerted a smaller impact on [LA] time-course profiles (Fig. 8) and had a relatively small but consistent effect on d[LA]/dt (Fig. 9). For formulations with identical [mAb] and initial [PS20], d[LA]/dt was slightly higher for pH 6

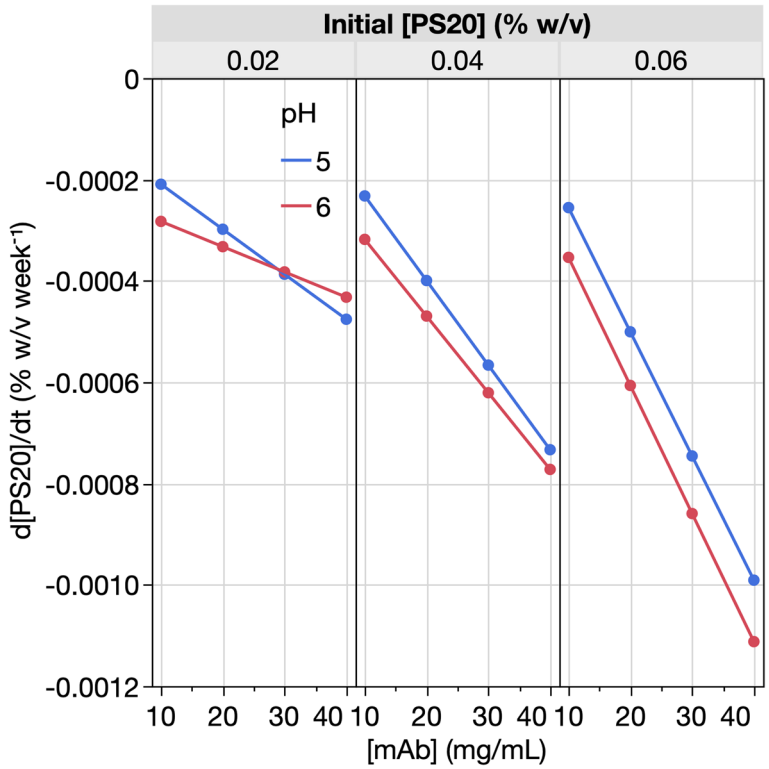

Fig. 7 Rate of change in [PS20] as a function of [mAb] in mAb X DP stored at 5 °C. The 24 formulations (listed in Table 1) represent unique combinations of [mAb], initial [PS20], and pH. Intact [PS20] remaining in each formulation at 12 time points over 24 weeks was quantified by HPLC-ELSD. The rate of change in PS20 concentration (d[PS20]/dt) was calculated as the derivative from fitting the longitudinal model

compared to pH 5, complementing the general observations for d[PS20]/dt (Fig. 7). Taken together, these results indicate that the PS20 degradation over DP storage at 5 °C for mAb X formulations tends to be marginally higher at pH 6 for the aforementioned potential reasons discussed in the previous section on PS20 concentration.

Correlations between PS20 and free fatty acid (FFA) concentrations

Over 5 °C DP storage duration, the 24 formulations were tested for intact [PS20] (Fig. 6) and [FFA] (with [LA] shown in Fig. 8). The formulations showed a negative correlation between [PS20] and [LA], with a clear separation based on the initial [PS20] (Fig. 10). The strong negative linear correlations are consistent with the PS20 degradation mechanism in mAb X formulations being hydrolytic instead of oxidative in nature.

MA is expected to be the next most abundant FFA degradant from PS20 hydrolysis, after LA; PA and SA are also expected to be generated upon PS20 hydrolysis, but at much lower levels than LA and MA (Doshi et al. 2020, 2021). To assess for correlations between the [PS20] and the concentration of PS20 degradants (i.e., [FFA]), scatterplot matrices for [PS20], [LA], [MA], [PA], and [SA] were generated. Correlations for the formulations with mid-range initial [PS20] (0.04% w/v) are displayed in Fig. 11. At the lower and higher initial [PS20] (0.02% w/v and 0.06% w/v), similar correlations were observed (Supplementary Figs. S6 and S7).

Correlations observed here between [PS20] and the concentration of PS20 degradants ([LA], [MA], [PA], and [SA]) demonstrate the potential for PS20 and FFA measurements as orthogonal and complementary analytical techniques for assessing PS20 hydrolytic degradation. Meanwhile, correlations across the FFAs demonstrate the feasibility of using trends in [LA] to approximate trends in [MA], [PA], and [SA] during PS20 hydrolysis. Since LA is present at a significantly higher level than the other FFAs, it can be quantified more readily above background noise and with greater precision by the LC–MS analytical method (Honemann et al. 2019). Therefore, out of all the FFAs, [LA] is expected to show the strongest correlation with [PS20] in terms of change over DP storage. This expectation is consistent with the higher correlation values observed for [PS20] with [LA] than for [PS20] with [MA], [PA]

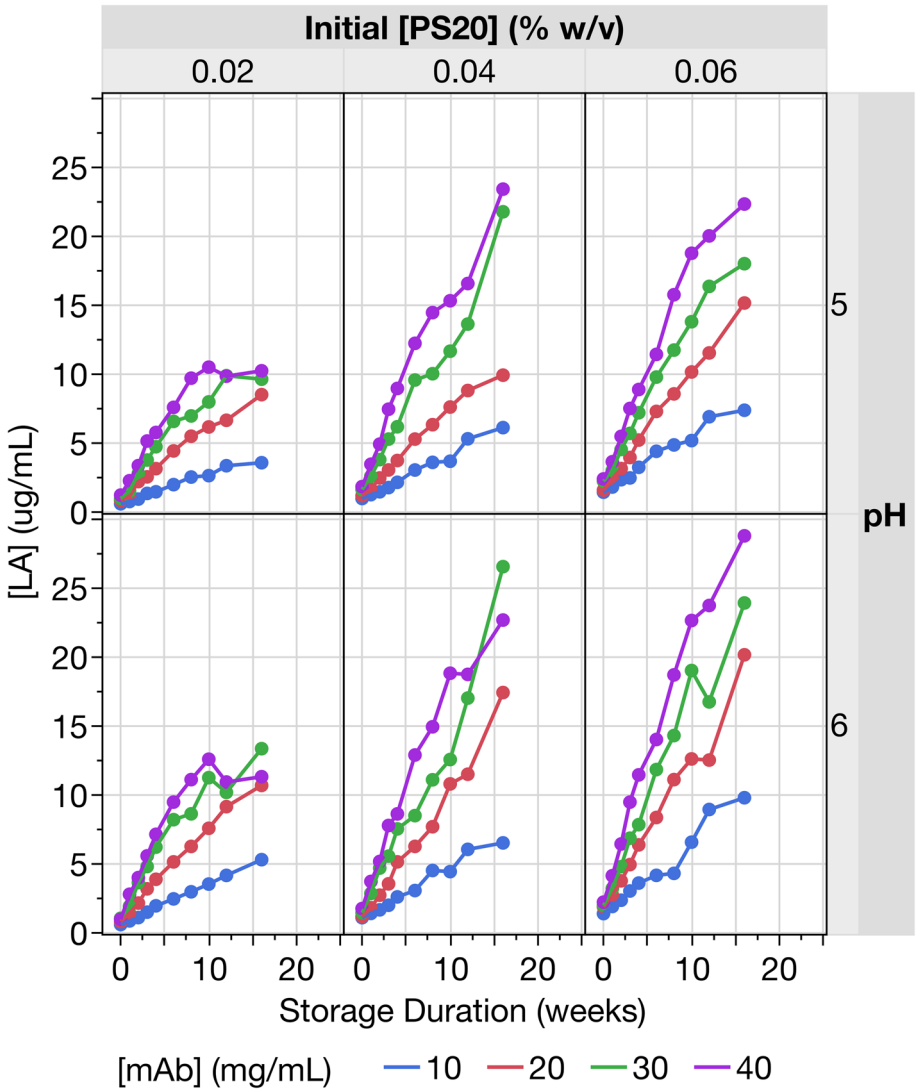

Fig. 8 [LA] in mAb X DP over storage duration (weeks at 5 °C). The 24 formulations (listed in Table 1) represent unique combinations of [mAb], initial [PS20], and pH. LA represents the most abundant degradant from PS20 hydrolysis. [LA] in each formulation was quantified by LC–MS

or [SA], as shown for 0.04% w/v initial [PS20] (Fig. 11), and also observed for 0.02% w/v initial [PS20] (Supplementary Fig. S6) and 0.06% w/v initial [PS60] (Supplementary Fig. S7).

Free fatty acid (FFA) solubility model

Comparison of model predictions with experimental observations

After establishing the empirical relationship for the solubility limits of the three predominant FFAs (namely LA, MA, and PA) released by PS20 degradation as a function of pH and initial [PS20] in a liquid formulation (Doshi et al. 2015), the FFA solubility model was recently updated (Doshi et al. 2020). This update incorporates the impact of PS20 ester distribution of the remaining intact PS20 on the solubility of each FFA—and accounts for the stronger solubilizing capacity for FFAs by higher order esters than monoesters. Hence, this update can also account for the impact of different hydrolytic enzymes if they show different PS20 ester substrate specificities (Graf et al. 2020; McShan et al. 2016).

By measuring the intact [PS20] and PS20 ester distribution in the samples, the projected solubility limits for three main FFA degradants from PS20 hydrolysis—LA, MA, and PA—were calculated using the FFA solubility model (Doshi et al. 2020) at each formulation pH over the longitudinal study. These calculations indicate the risks of these FFAs exceeding their respective solubility limits during the course of the study. Only the lowest and highest [mAb] were selected (10 mg/mL and 40 mg/mL)

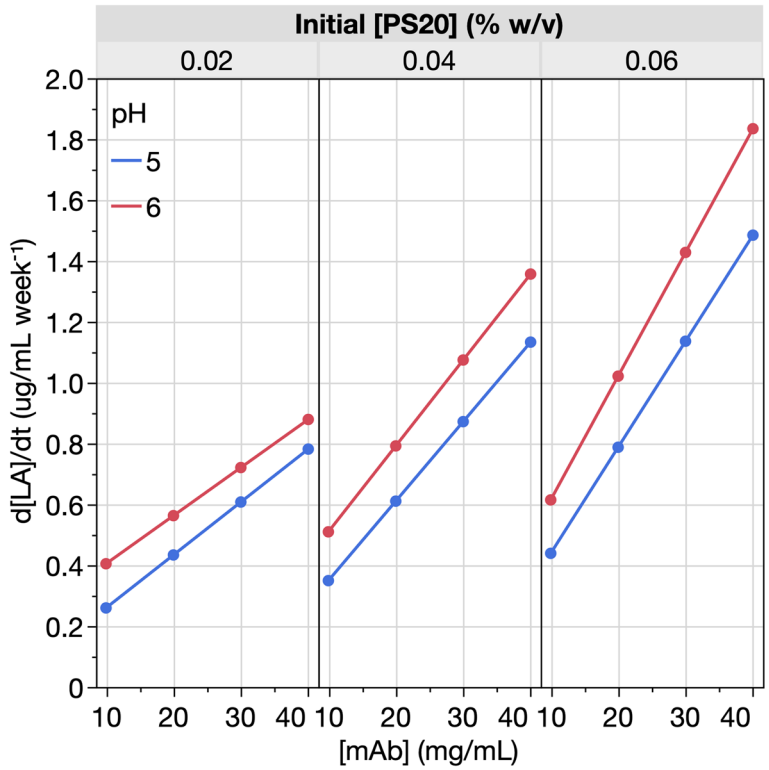

Fig. 9 Rate of change in [LA] as a function of [mAb] in mAb X DP stored at 5 °C. The 24 formulations (listed in Table 1) represent unique combinations of [mAb], initial [PS20], and pH. LA represents the most abundant degradant from PS20 hydrolysis. [LA] in each formulation was quantified by LC–MS. The rate of change in LA concentration (d[LA]/dt) was calculated as the derivative from fitting the longitudinal model

to provide critical information on the impact of [mAb]. The intermediate [mAb] (20 mg/mL and 30 mg/mL) were omitted to reduce the analytical testing burden for PS20 ester distribution while retaining a full-factorial design for the three key formulation parameters.

The presence of PS20 surfactant in each formulation imparts solubilizing capacity towards FFAs. Accordingly, higher [PS20] in a formulation would increase the FFA solubility limit (Doshi et al. 2015). Over time, the calculated FFA solubility limits are projected to decline because of the corresponding PS20 degradation that lowers the FFA-solubilizing capacity of the formulation. The more rapid decline in FFA solubility limit at the highest [mAb] relative to the lowest [mAb] (Fig. 12) is consistent with the more rapid decline in [PS20] at higher [mAb] (Figs. 6 and 7).

The predictions from the FFA solubility model were compared against the empirical observations for each formulation (Fig. 12). In the top three panels, the blue hollow circles (and associated blue lines) denote the calculated solubility limits for LA, MA, and PA, while the red filled circles (and associated red lines) denote the measured concentrations of these three FFAs. For a given formulation, the intersection of the blue and red lines represents the time point where the measured FFA concentration reached its calculated solubility limit and the FFA is expected to thereafter fall out of solution and precipitate as FFA particles (Fig. 12, top 3 panels). The expected VP onset from the FFA solubility model for LA, MA, and PA corroborated the general VP and SVP trends observed in this longitudinal DOE study: (1) lower [mAb] extended VP-free duration; (2) higher initial [PS20] extended VP-free duration; (3) pH had minimal impact.

The solubility for LA, MA, and PA decreases in this order, in an inverse relationship to their chain lengths (Doshi et al. 2020). Therefore, PA has the lowest calculated solubility limit of the three FFAs. PA is also projected to accumulate beyond its solubility limit at earlier time points than LA and MA and thereby precipitate earlier. In Fig. 12, the intersections of the blue and red lines for PA (third panel from top) occur at earlier time points relative to LA (top panel) and MA (second panel from top), thereby indicating that the long-chain FFAs like PA are likely the root cause for the onset of particles. In the bottom panel of Fig. 12, the first time points where VPs were observed are denoted by green asterisks and the rise

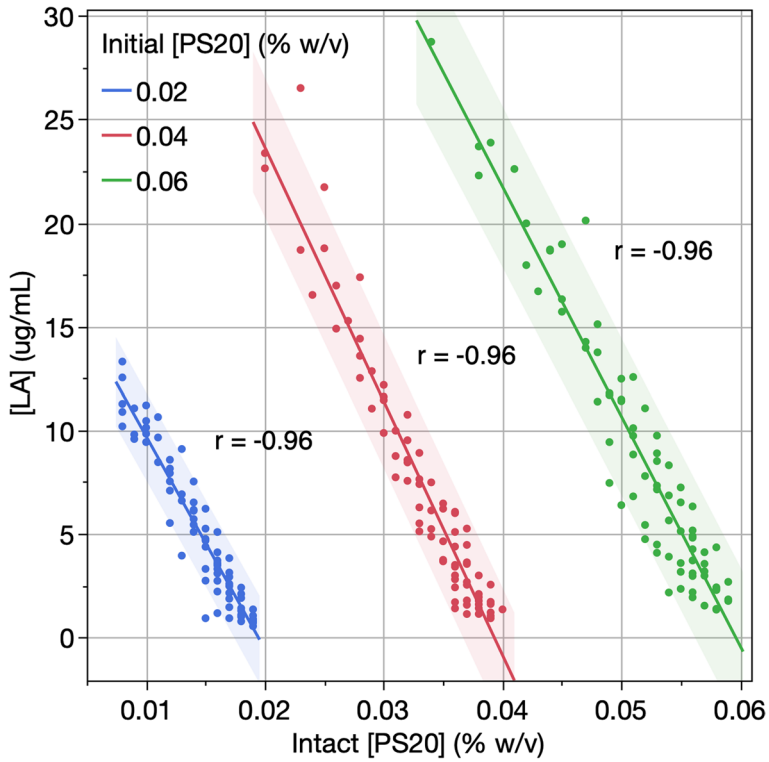

Fig. 10 Correlations between [LA] and intact [PS20] for mAb X DP stored at 5 °C. The 24 formulations (listed in Table 1) represent unique combinations of [mAb], initial [PS20], and pH. [LA] was quantified by LC–MS; intact [PS20] was quantified by HPLC-ELSD. Correlation coefficient (*r*) values for formulations with the same initial [PS20] are shown within the plot. Shaded areas represent 95% prediction intervals of the fitted lines

in SVP counts is shown by the black filled diamonds (and associated black lines).

The pH of the formulation impacts the LA solubility limits—pH 6 has a higher predicted LA solubility relative to pH 5 (Fig. 12). By contrast, pH has minimal impact on the predicted solubility limits of MA and PA. The higher LA solubility limit at pH 6 relative to pH 5 is attributed to the increased proportion of ionized LA—which is significantly more soluble than its non-ionized form—in the pH 6 formulations (Doshi et al. 2015). Owing to their high pKas (>7), the ratio of ionized to non-ionized FFA does not change much for MA and PA in the pH range of 5–6, which explains the minimal impact of pH on their solubility limits (Doshi et al. 2015). This observation also supports the hypothesis that the longer chain FFAs such as PA are likely the key contributors to particle onset since pH had a minimal impact on SVP and VP formation in this study.

A key limitation of the FFA solubility model is its lack of SA coverage. SA is too insoluble for SA solutions to be prepared for the necessary empirical studies to establish the FFA solubility model. Some SA is expected to be generated from PS20 degradation because typically a small proportion of compendial-grade PS20 is composed of SA esters (Doshi et al. 2015). SA was indeed detected in the formulation samples, albeit at very low concentrations (Fig. 10). Since SA is less soluble than PA, SA may precipitate earlier than PA in these formulations. In other in-house studies, VPs that formed earliest were comprised primarily of SA and PA, whereas VPs that formed later included MA with SA and PA in its composition (Saggu et al. 2021). Another limitation of the FFA solubility model is its lack of coverage for nucleation factors, which have been shown to trigger the onset of VPs below predicted FFA solubility limits (Allmendinger et al. 2021; Gregoritza et al. 2022). In spite of these limitations, the FFA solubility model increased our understanding of the observed impact of the formulation parameters on VP outcomes in the ranges tested in this longitudinal DoE study.

Statistical analysis of formulation parameter effects

This longitudinal DoE study was designed to facilitate statistical analysis on the quantitative impact of each of the three formulation parameters—[mAb], initial [PS20], and pH—and their interactions on particle formation and PS20 degradation in mAb X drug product over real-time stability (i.e., DP storage at 5 °C). By

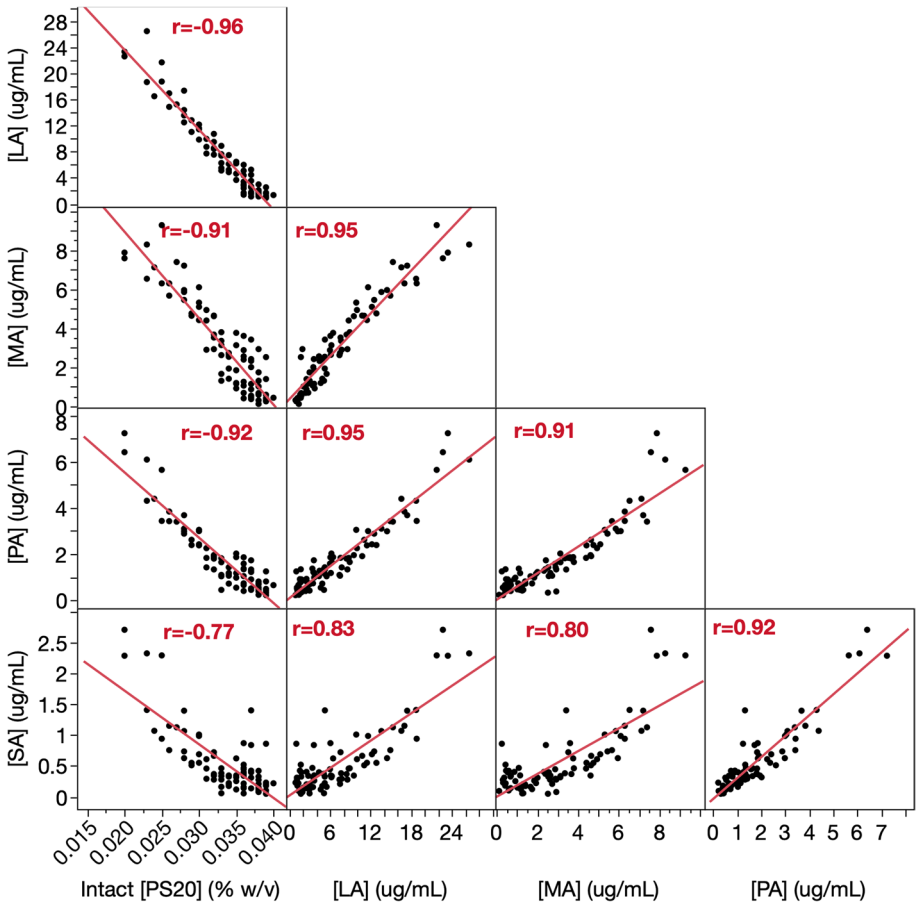

Fig. 11 Correlations between intact [PS20], [LA], [MA], [PA], and [SA] in mAb X DP formulations stored at 5 °C. Formulations shown here contain the same initial [PS20] (0.04% w/v) paired with unique combinations of [mAb] and pH. Intact PS20 was quantified by HPLC-ELSD; FFAs were quantified by LC–MS. Correlation coefficient (*r*) values are shown within the scatterplot matrix

applying the longitudinal model of the data, with the formulation parameters coded to the lowest and highest values tested, effect estimates were determined for particle outcomes—based on duration with no VPs and duration with low SVP counts (Eq. 2). By taking the derivatives to fit the longitudinal model (Eq. 1), effect estimates were determined for rates of PS20 degradation—based on longitudinal data for [PS20] and [LA]. This DoE approach empowered the comprehensive and systematic analysis of each formulation parameter and potential interactions of these parameters relating to PS20 degradation and particle formation as a function of time. The quality of the model fits was assessed using actual-by-predicted scatterplots (Supplementary Fig. S8), where the observed data were plotted against the predicted values that were derived from the model fits. The actual-by-predicted plots demonstrate that predicted values agree with the observed values on average. The resulting *R*-squared (R^2) values for each fit were as follows: (a) low SVP duration: 0.896; (b) VP-free duration: 0.901; (c) intact [PS20]: 0.995; and (d) [LA]: 0.961.

[mAb] exerted the largest effect on all the outputs assessed for both particle formation and rate of PS20 degradation, demonstrated by the largest absolute values calculated for its effect estimates (Table 2). The initial [PS20] exerted the next largest effect estimate across all outputs. The beneficial effect of higher initial [PS20] in extending both VP-free duration and low SVP duration demonstrates that the higher FFA-solubilizing capacity at higher initial [PS20] more than offset the correspondingly higher rate of PS20 degradation and FFA generation in mAb X DP. Based on the longitudinal model, the effect estimates for the interaction between [mAb] and initial [PS20] exceeded the effect estimates for pH on

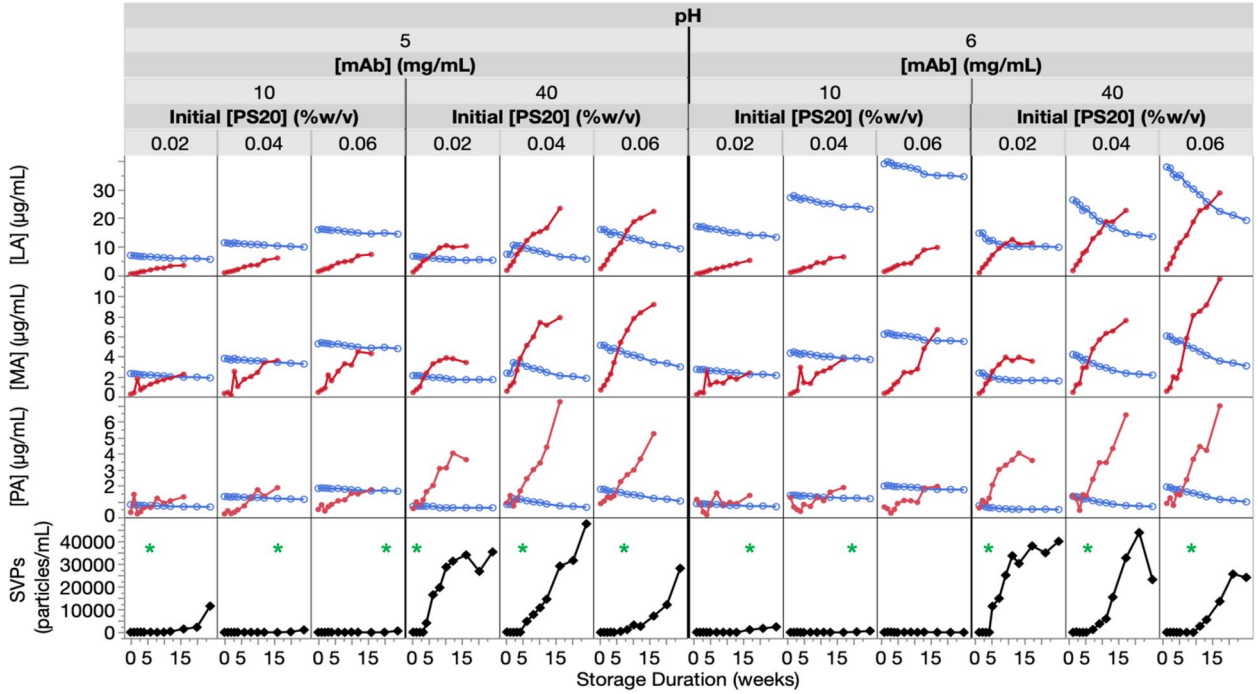

Fig. 12 Comparison of calculated FFA solubility limits (blue hollow circles) with corresponding FFA measurements (red filled circles), SVP counts (black filled diamonds), and VP observations (green asterisks) in mAb X DP stored at 5 °C. FFA solubility limits at the different time points for each formulation were calculated using the updated FFA solubility model by Doshi et al. (Doshi et al. 2020). Formulations were analyzed for LA, MA, and PA (by LC–MS), cumulative SVPs (≥ 2 µm particles/mL by HIAC), and VPs (by the Ph. Eur./USP method). Green asterisks (bottom panel) denote the earliest time points at which VPs were observed for the given formulation (Table 1)

all the outputs (Table 2). The [mAb] × initial [PS20] interaction is also manifested in the observed differences in slopes at the different initial [PS20] for the following four outputs: (1) VP-free duration (Fig. 2); (2) low SVP duration (Fig. 4); (3) d[PS20]/dt with [mAb] (Fig. 7); and (4) d[LA]/dt with [mAb] (Fig. 9). By contrast, the slopes for pH 5 and pH 6 formulations across these four outputs were relatively similar within the same initial [PS20] (Figs. 2, 4, 7, and 9), consistent with the relatively small effect estimates for pH and its interaction with the other formulation parameters on particle formation and PS20 degradation (Table 2).

The large effect of [mAb] on accelerating PS20 degradation and particle formation in mAb X DP substantiates the premise that these important DP stability attributes are negatively impacted by the industry trend of formulating DPs at higher concentrations. The UFDF process used to concentrate the mAb is expected to concomitantly concentrate residual HCPs and thereby elevate the total enzymatic activity towards polysorbate degradation in the DP. Hence, the large effect of [mAb] on PS20 degradation and particle outcomes for mAb X DP corroborates the overall causal relationships: (1) residual hydrolytic HCPs in DP degrade polysorbate to release FFAs; (2) accumulation of FFAs over storage time eventually lead to FFA particles when FFA solubility limits are exceeded; and therefore (3) increasing [mAb] in DP would accelerate and amplify polysorbate degradation and particle formation.

The general trends observed here for the impact of [mAb] and initial [PS20] on PS20 degradation and FFA particle formation in mAb X DP are also expected to be observed when [mAb] is replaced by other types of recombinant protein concentration and/or PS20 is replaced by PS80. In theory, the concepts explored here should apply for other recombinant protein-based DPs containing polysorbate, irrespective of the identity of the recombinant protein or the type of polysorbate (PS20 or PS80). The concentration of residual HCPs in a therapeutic protein product is expected to increase with protein concentration if no bioprocess changes (apart from concentrating the product) are made to the upstream and downstream steps for protein production and purification.

Table 2 Effect estimates for three formulation parameters and their interactions on particle formation and PS20 degradation. The formulation parameters—[mAb], initial [PS20], and pH—were tested in a DP stability study at 5 °C with a full-factorial design. Particle formation was evaluated as duration with no VPs (by the Ph. Eur./USP method) and duration with low SVPs (< 350 counts for ≥ 2 µm particles/mL by HIAC liquid particle counter). PS20 degradation was quantified by measuring [PS20] in % w/v by HPLC-ELSD (Fig. 6) and [LA] in µg/mL by LC–MS (Fig. 8) over DP storage. The rate of PS20 change (d[PS20]/dt; Fig. 7) and rate of LA change (d[LA]/dt; Fig. 9) were calculated using the derivatives from fitting to a longitudinal model

Formulation parameters				Effect estimates (midpoint to high end of range)			
				Duration (weeks)		Rate ($week^{-1}$)	
Parameter(s) (units)		Term	Coded range	No VPs	Low SVPs	d[PS20]/dt($\times 10^{-4}$)	d[LA]/dt
Main effects	mAb concentration (mg/mL)	[mAb]	10–40	−5.95*	−6.78*	−2.39*	0.41*
	Initial PS20 concentration (% w/v)	Initial [PS20]	0.02–0.06	3.88*	4.19*	−1.64*	0.26*
	pH	pH	5.0–6.0	0.50	0.38	−0.31*	0.10*
Interactions	mAb concentration (mg/mL) and initial PS20 concentration (% w/v)	[mAb] × initial [PS20]	10–40; 0.02–0.06	−1.88*	−2.44*	−1.35*	0.16*
	mAb concentration (mg/mL) and pH	[mAb] × pH	10–40; 5.0–6.0	−0.50	0.13	0.12	0.02
	Initial PS20 concentration (% w/v) and pH	Initial [PS20] × pH	0.02–0.06; 5.0–6.0	0.25	0.19	−0.24*	0.04
	mAb concentration (mg/mL), initial PS20 concentration (% w/v), and pH	[mAb] × initial [PS20] × pH	10–40; 0.02–0.06; 5.0–6.0	0.15	0.41	−0.18	0.03

* p-value < 0.05

Glucklich et al. recently developed FFA solubility models that corroborated our model for key FFAs released by PS20 hydrolysis (Doshi et al. 2015) and added a new model to include the key FFAs (OA, PA, and SA) released by PS80 hydrolysis; their models for both PS20 and PS80 FFA degradants show that FFA solubilities increase with higher [PS20] or [PS80] (Glücklich et al. 2020).

Conclusions

This longitudinal DoE study conducted with mAb X DP at the representative stability condition of 5 °C underscores the considerable impact of two key formulation parameters—[mAb] and initial [PS20]—on particle formation and PS20 degradation. By applying statistical analysis to the outputs generated by our state-of-the-art analytical toolbox, this comprehensive study supports the following conclusions for liquid DPs formulated with PS20 as the surfactant: (1) The shift to higher [mAb] is substantiated as a leading root cause for the increasing prevalence of FFA particle observations across the biopharmaceutical industry. (2) The risk of FFA particle formation is further exacerbated when the increase in [mAb] is not counteracted by an increase in the initial [PS20] to enhance the FFA-solubilizing capacity of the formulation. (3) The effect of formulation pH in the 5–6 range is considerably less than the effect of [mAb] or initial [PS20] or the interaction of [mAb] and initial [PS20]. (4) The observed VP trends are consistent with the predictions by our updated FFA solubility model (Doshi et al. 2020). In summary, to mitigate particle formation in DP formulated with PS20, the alternatives to consider—apart from shortening DP shelf-life or optimizing drug substance process to minimize levels of residual hydrolytic HCPs—are to decrease [mAb] and/or increase initial [PS20].

Abbreviations

2DLC: Two-dimensional liquid chromatography; CAD: Charged aerosol detector; CQA: Critical quality attribute; d[LA]/dt: Rate of change in lauric acid concentration; DoE: Design of Experiments; DP: Drug product; d[PS20]/dt: Rate of change in PS20 concentration; |d[PS20]/dt|: Absolute value of rate of change in PS20 concentration; ELSD: Evaporative light scattering detector; FFA: Free fatty acid; [FFA]: Free fatty acid concentration; HCP: Host cell protein; HPLC: High-performance liquid chromatography; LA: Lauric acid; [LA]: Lauric acid concentration; LC-MS: Liquid chromatography-mass spectrometry; mAb: Monoclonal antibody; [mAb]: Monoclonal antibody concentration; MA: Myristic acid; [MA]: Myristic acid concentration; OA: Oleic acid; PA: Palmitic acid; [PA]: Palmitic acid concentration; Ph. Eur. : European Pharmacopoeia; PS20: Polysorbate 20; [PS20]: Polysorbate 20 concentration; PS80: Polysorbate 80; [PS80]: Polysorbate 80 concentration; r: Correlation coefficient; R^2: Coefficient of determination; REML: Restricted maximum likelihood; SA: Stearic acid; [SA]: Stearic acid concentration; SVP: Subvisible particle; USP: United States Pharmacopoeia; V_{max}: Maximum rate of enzymatic reaction at substrate saturation; VP: Visible particle.

Supplementary Information

The online version contains supplementary material available at https://doi.org/10.1186/s41120-022-00064-3.

Additional file 1: Supplementary Figure S1. Cumulative SVP counts (≥5 µm particles/mL) measured in mAb X DP over storage duration (weeks at 5°C). Three formulation parameters—[mAb], initial [PS20] and pH—were assessed for their impact on SVP accumulation as measured by HIAC liquid particle counter. The 24 formulations and their VP outcomes are detailed in Table 1. Colored asterisks in the plots denote the earliest time points at which VPs were observed for the formulation (with corresponding [mAb] represented by the same color).

Additional file 2: Supplementary Figure S2. Cumulative SVP counts (≥10 µm particles/mL) measured in mAb X DP over storage duration (weeks at 5°C). Three formulation parameters—[mAb], initial [PS20] and pH—were assessed for their impact on SVP accumulation as measured by HIAC liquid particle counter. The 24 formulations and their VP outcomes are detailed in Table 1. Colored asterisks in the plots denote the earliest time points at which VPs were observed for the formulation (with corresponding [mAb] represented by the same color).

Additional file 3: Supplementary Figure S3. Cumulative SVP counts (≥25 µm particles/mL) measured in mAb X DP over storage duration (weeks at 5°C). Three formulation parameters—[mAb], initial [PS20] and pH—were assessed for their impact on SVP accumulation as measured by HIAC liquid particle counter. The 24 formulations and their VP outcomes are detailed in Table 1. Colored asterisks in the plots denote the earliest time points at which VPs were observed for the formulation (with corresponding [mAb] represented by the same color).

Additional file 4: Supplementary Figure S4. Representative 2DLC CAD chromatograms of PS20 ester distribution at different storage durations (weeks at 5°C). The PS20 monoester and higher order ester peak areas are demarcated by the vertical dashed line. The chromatograms represent PS20 ester distribution in F9 formulation (as listed in Table 1) at 0 weeks (in blue) and then after 24 weeks (in black) at 5°C.

Additional file 5: Supplementary Figure S5. PS20 higher order ester peak area (%) measured in mAb X DP formulations (with [mAb] at 10 and 40 mg/mL) over storage duration (weeks at 5°C). Three formulation parameters—[mAb]), initial [PS20] and pH—were assessed for their impact on % higher order ester peak area in PS20 as measured by 2DLC CAD. The % monoester peak area is calculated as 100 - % higher order ester peak area.

Additional file 6: Supplementary Figure S6. Correlations between intact [PS20], [LA], [MA], [PA], and [SA] in mAb X DP formulations stored at 5°C. Formulations shown here contain the same initial [PS20] (0.02% w/v) paired with unique combinations of [mAb] and pH. Intact PS20 was quantified by HPLC-ELSD; FFAs were quantified by LC-MS. Correlation coefficient (r) values are shown within the scatterplot matrix.

Additional file 7: Supplementary Figure S7. Correlations between intact [PS20], [LA], [MA], [PA], and [SA] in mAb X DP formulations stored at 5°C. Formulations shown here contain the same initial [PS20] (0.06% w/v) paired with unique combinations of [mAb] and pH. Intact PS20 was quantified by HPLC-ELSD; FFAs were quantified by LC-MS. Correlation coefficient (r) values are shown within the scatterplot matrix.

Additonal file 8: Supplementary Figure S8. Actual-by-Predicted plots for low SVP duration, VP-free duration, intact [PS20] and [LA]. Predicted values are based on model fits of equation (2) for (a) low SVP duration and (b) VP-free duration, and model fits of equation (1) for (c) intact [PS20] and (d) [LA].

Acknowledgements
We would like to thank Cosimo Pinto, Christoph Paschen, and Heinrich Furlenmeier for performing the PS20 quantification.

Authors' contributions
TAK conceptualized the study design. IHY wrote the manuscript. TK performed the statistical analysis of the data. CH prepared the formulations, managed the stability samples, and performed the particulate analytics. VLH performed the FFA quantification and JG performed PS20 ester distribution characterization. IHY, TK, ND, KG, and TAK analyzed/interpreted the data and provided a critical review of the manuscript. The authors read and approved the final manuscript.

Funding
Not applicable.

Availability of data and materials
All data generated or analyzed during this study are included in this published article and its supplementary information files.

Declarations

Competing interests
The authors declare that they have no competing interests.

Author details
[1]Pharma Technical Development US, Genentech Inc., 1 DNA Way, South San Francisco, CA 94080, USA. [2]Nonclinical Biostatistics, Product Development, US, Genentech Inc., 1 DNA Way, South San Francisco, CA 94080, USA. [3]Pharma Technical Development Europe, F. Hoffmann-La Roche Ltd., Grenzacherstrasse 124, 4070 Basel, Switzerland.

Received: 26 April 2022 Accepted: 29 September 2022
Published online: 14 November 2022

References

Allmendinger A, Lebouc V, Bonati L, Woehr A, Kishore RS, Abstiens K (2021) Glass leachables as a nucleation factor for free fatty acid particle formation in biopharmaceutical formulations. J Pharm Sci 110(2):785–795
Bar-Even A, Milo R, Noor E, Tawfik DS (2015) The moderately efficient enzyme: futile encounters and enzyme floppiness. Biochemistry 54(32):4969–4977
Bengtsson G, Olivecrona T (1980) Lipoprotein lipase: mechanism of product inhibition. Eur J Biochem 106(2):557–562
Bengtsson G, Olivecrona T (1982) On the pH dependency of lipoprotein lipase activity. Biochim Biophys Acta 712(1):196–199
Bhargava AC, Mains K, Siu A, Gu J, Zarzar J, Yi L, Yuk IH (2021) High-throughput, fluorescence-based esterase activity assay for assessing polysorbate degradation risk during biopharmaceutical development. Pharm Res 38(3):397–413
Cao X, Fesinmeyer RM, Pierini CJ, Siska CC, Litowski JR, Brych S, Wen Z-Q, Kleemann GR (2015) Free fatty acid particles in protein formulations, part 1: microspectroscopic identification. J Pharm Sci 104(2):433–446
Carpenter JF, Randolph TW, Jiskoot W, Crommelin DJ, Middaugh CR, Winter G, Fan Y-X, Kirshner S, Verthelyi D, Kozlowski S (2009) Overlooking subvisible particles in therapeutic protein products: gaps that may compromise product quality. J Pharm Sci 98(4):1201–1205
Chiu J, Valente KN, Levy NE, Min L, Lenhoff AM, Lee KH (2017) Knockout of a difficult-to-remove CHO host cell protein, lipoprotein lipase, for improved polysorbate stability in monoclonal antibody formulations. Biotechnol Bioeng 114(5):1006–1015
Corvari V, Narhi LO, Spitznagel TM, Afonina N, Cao S, Cash P, Cecchini I, DeFelippis MR, Garidel P, Herre A (2015) Subvisible (2–100 µm) particle analysis during biotherapeutic drug product development: part 2, experience with the application of subvisible particle analysis. Biologicals 43(6):457–473
Dixit N, Salamat-Miller N, Salinas PA, Taylor KD, Basu SK (2016) Residual host cell protein promotes polysorbate 20 degradation in a sulfatase drug product leading to free fatty acid particles. J Pharm Sci 105(5):1657–1666
Doessegger L, Mahler H-C, Szczesny P, Rockstroh H, Kallmeyer G, Langenkamp A, Herrmann J, Famulare J (2012) The potential clinical relevance of visible particles in parenteral drugs. J Pharm Sci 101(8):2635–2644
Doshi N, Bl D, Yadav S (2015) Understanding particle formation: solubility of free fatty acids as polysorbate 20 degradation byproducts in therapeutic monoclonal antibody formulations. Mol Pharm 12(11):3792–3804

Doshi N, Martin J, Tomlinson A (2020) Improving prediction of free fatty acid particle formation in biopharmaceutical drug products: incorporating ester distribution during polysorbate 20 degradation. Mol Pharm 17(11):4354–4363

Doshi N, Ritchie K, Shobha T, Giddings J, Gregoritza K, Taing R, Rumbelow S, Chu J, Tomlinson A, Kannan A (2021) Evaluating a modified high purity polysorbate 20 designed to reduce the risk of free fatty acid particle formation. Pharm Res 38(9):1563–1583

Dwivedi M, Blech M, Presser I, Garidel P (2018) Polysorbate degradation in biotherapeutic formulations: identification and discussion of current root causes. Int J Pharm 552(1–2):422–436

Dwivedi M, Buske J, Haemmerling F, Blech M, Garidel P (2020) Acidic and alkaline hydrolysis of polysorbates under aqueous conditions: towards understanding polysorbate degradation in biopharmaceutical formulations. Eur J Pharm Sci 144:105211

Falconer RJ (2019) Advances in liquid formulations of parenteral therapeutic proteins. Biotechnol Adv 37(7):107412

Fitzmaurice GM, Laird NM, Ware JH (2011) Applied longitudinal analysis, vol 998. John Wiley & Sons, Hokoken, NJ, USA

Gervasi V, Agnol RD, Sa C, McCoy T, Vucen S, Crean A (2018) Parenteral protein formulations: an overview of approved products within the European Union. Eur J Pharm Biopharm 131:8–24

Glücklich N, Dwivedi M, Carle S, Buske J, Mäder K, Garidel P (2020) An in-depth examination of fatty acid solubility limits in biotherapeutic protein formulations containing polysorbate 20 and polysorbate 80. Int J Pharm 591:119934

Graf T, Abstiens K, Wedekind F, Elger C, Haindl M, Wurth C, Leiss M (2020) Controlled polysorbate 20 hydrolysis–a new approach to assess the impact of polysorbate 20 degradation on biopharmaceutical product quality in shortened time. Eur J Pharm Biopharm 152:318–326

Graf T, Tomlinson A, Yuk IH, Kufer R, Spensberger B, Falkenstein R, Shen A, Li H, Duan D, Liu W (2021) Identification and characterization of polysorbate-degrading enzymes in a monoclonal antibody formulation. J Pharm Sci 110(11):3558–3567

Gregoritza K, Cai SK, Siketanc M, Woehr A, Lebouc V, Kishore RS, Nicoulin V, Bleher S, Allmendinger A (2022) Metal-induced fatty acid particle formation resulting from hydrolytic polysorbate degradation. J Pharm Sci 111(3):743–751

Guha MK, Vander Jagt DL, Creighton DJ (1988) Diffusion-dependent rates for the hydrolysis reaction catalyzed by glyoxalase II from rat erythrocytes. Biochemistry 27(24):8818–8822

Hall T, Sandefur SL, Frye CC, Tuley TL, Huang L (2016) Polysorbates 20 and 80 degradation by group XV lysosomal phospholipase A2 isomer X1 in monoclonal antibody formulations. J Pharm Sci 105(5):1633–1642

Hewitt D, Zhang T, Kao Y-H (2008) Quantitation of polysorbate 20 in protein solutions using mixed-mode chromatography and evaporative light scattering detection. J Chromatogr A 1215(1–2):156–160

Hewitt D, Alvarez M, Robinson K, Ji J, Wang YJ, Kao Y-H, Zhang T (2011) Mixed-mode and reversed-phase liquid chromatography–tandem mass spectrometry methodologies to study composition and base hydrolysis of polysorbate 20 and 80. J Chromatogr A 1218(15):2138–2145

Honemann MN, Wendler J, Graf T, Bathke A, Bell CH (2019) Monitoring polysorbate hydrolysis in biopharmaceuticals using a QC-ready free fatty acid quantification method. J Chromatogr B 1116:1–8

Ichihara T, Ito T, Kurisu Y, Galipeau K, Gillespie C (2018) Integrated flow-through purification for therapeutic monoclonal antibodies processing. Mabs 10(2):325–334

Ichihara T, Ito T, Gillespie C (2019) Polishing approach with fully connected flow-through purification for therapeutic monoclonal antibody. Eng Life Sci 19:31–36

Imai T (2006) Human carboxylesterase isozymes: catalytic properties and rational drug design. Drug Metab Pharmacokinet 21(3):173–185

Jones MT, Mahler H-C, Yadav S, Bindra D, Corvari V, Fesinmeyer RM, Gupta K, Harmon AM, Hinds KD, Koulov A (2018) Considerations for the use of polysorbates in biopharmaceuticals. Pharm Res 35(8):1–8

Khan TA, Mahler H-C, Kishore RS (2015) Key interactions of surfactants in therapeutic protein formulations: a review. Eur J Pharm Biopharm 97:60–67

Kishore RS, Kiese S, Fischer S, Pappenberger A, Grauschopf U, Mahler H-C (2011a) The degradation of polysorbates 20 and 80 and its potential impact on the stability of biotherapeutics. Pharm Res 28(5):1194–1210

Kishore RS, Pappenberger A, Dauphin IB, Ross A, Buergi B, Staempfli A, Mahler H-C (2011b) Degradation of polysorbates 20 and 80: studies on thermal autoxidation and hydrolysis. J Pharm Sci 100(2):721–731

Kranz W, Wuchner K, Corradini E, Berger M, Hawe A (2019) Factors influencing polysorbate's sensitivity against enzymatic hydrolysis and oxidative degradation. J Pharm Sci 108(6):2022–2032

Labrenz SR (2014) Ester hydrolysis of polysorbate 80 in mAb drug product: evidence in support of the hypothesized risk after the observation of visible particulate in mAb formulations. J Pharm Sci 103(8):2268–2277

Li Y, Hewitt D, Lentz YK, Ji JA, Zhang TY, Zhang K (2014) Characterization and stability study of polysorbate 20 in therapeutic monoclonal antibody formulation by multidimensional ultrahigh-performance liquid chromatography–charged aerosol detection–mass spectrometry. Anal Chem 86(10):5150–5157

Lippold S, Koshari SH, Kopf R, Schuller R, Buckel T, Zarraga IE, Koehn H (2017) Impact of mono-and poly-ester fractions on polysorbate quantitation using mixed-mode HPLC-CAD/ELSD and the fluorescence micelle assay. J Pharm Biomed Anal 132:24–34

McShan AC, Kei P, Ji JA, Kim DC, Wang YJ (2016) Hydrolysis of polysorbate 20 and 80 by a range of carboxylester hydrolases. PDA J Pharm Sci Technol 70(4):332–345

Page S, Khan T, Kühl P, Schwach G, Storch K, Chokshi H (2022) Patient centricity driving formulation innovation: improvements in patient care facilitated by novel therapeutics and drug delivery technologies. Annu Rev Pharmacol Toxicol 62:341–363

Pegues MA, Szczepanek K, Sheikh F, Thacker SG, Aryal B, Ghorab MK, Wolfgang S, Donnelly RP, Verthelyi D, Rao VA (2021) Effect of fatty acid composition in polysorbate 80 on the stability of therapeutic protein formulations. Pharm Res 38(11):1961–1975

Pinheiro J, Bates D (2000) Mixed-effects models in S and S-PLUS. Statistics and computing, 1st edn. Springer, New York. https://doi.org/10.1007/b98882

Roy I, Patel A, Kumar V, Nanda T, Assenberg R, Wuchner K, Amin K (2021) Polysorbate degradation and particle formation in a high concentration mAb: formulation strategies to minimize effect of enzymatic polysorbate degradation. J Pharm Sci 110(9):3313–3323

Saggu M, Liu J, Patel A (2015) Identification of subvisible particles in biopharmaceutical formulations using Raman spectroscopy provides insight into polysorbate 20 degradation pathway. Pharm Res 32(9):2877–2888

Saggu M, Demeule B, Jiang L, Kammerer D, Nayak PK, Tai M, Xiao N, Tomlinson A (2021) Extended characterization and impact of visible fatty acid particles-a case study with a mAb product. J Pharm Sci 110(3):1093–1102

Schmidt A, Koulov A, Huwyler J, Mahler H-C, Jahn M (2020) Stabilizing polysorbate 20 and 80 against oxidative degradation. J Pharm Sci 109(6):1924–1932

Strickley RG, Lambert WJ (2021) A review of formulations of commercially available antibodies. J Pharm Sci 110(7):2590-2608. e2556

Strube J, Ditz R, Kornecki M, Huter M, Schmidt A, Thiess H, Zobel-Roos S (2018) Process intensification in biologics manufacturing. Chem Eng Process Process Intensif 133:278–293

Tomlinson A, Bl D, Lin B, Yadav S (2015) Polysorbate 20 degradation in biopharmaceutical formulations: quantification of free fatty acids, characterization of particulates, and insights into the degradation mechanism. Mol Pharm 12(11):3805–3815

Valente KN, Levy NE, Lee KH, Lenhoff AM (2018) Applications of proteomic methods for CHO host cell protein characterization in biopharmaceutical manufacturing. Curr Opin Biotechnol 53:144–150

Xu J, Xu X, Huang C, Angelo J, Oliveira CL, Xu M, Xu X, Temel D, Ding J, Ghose S (2020) Biomanufacturing evolution from conventional to intensified processes for productivity improvement: a case study. Mabs 12(1):1770669

Yao J, Dokuru DK, Noestheden M, Park SS, Kerwin BA, Jona J, Ostovic D, Reid DL (2009) A quantitative kinetic study of polysorbate autoxidation: the role of unsaturated fatty acid ester substituents. Pharm Res 26(10):2303–2313

Zhang S, Xiao H, Molden R, Qiu H, Li N (2020) Rapid polysorbate 80 degradation by liver carboxylesterase in a monoclonal antibody formulated drug substance at early stage development. J Pharm Sci 109(11):3300–3307

Zhang S, Xiao H, Li N (2021) Degradation of polysorbate 20 by sialate O-acetylesterase in monoclonal antibody formulations. J Pharm Sci 110(12):3866–3873

Zhang J, He J, Smith KJ (2022a) Fatty acids can induce the formation of proteinaceous particles in monoclonal antibody formulations. J Pharm Sci 111(3):655–662
Zhang S, Riccardi C, Kamen D, Reilly J, Mattila J, Bak H, Xiao H, Li N (2022b) Identification of the specific causes of polysorbate 20 degradation in monoclonal antibody formulations containing multiple lipases. Pharm Res 39(1):75–87

Publisher's Note